Lappeenranta University of Technology
School of Energy Systems
Degree Program in Nuclear Engineering

Dmitry Skripnikov

THE TITLE OF THE WORK – SPRAY DROPLET SIZE DISTRIBUTION MEASUREMENT

Examiners: Professor Juhani Hyvärinen

Supervisors: M.Sc. Lauri Pyy

ABSTRACT

Lappeenranta University of Technology
School of Energy Systems
Degree Program in Nuclear Engineering

Dmitry Skripnikov

Title of the work – Spray droplet size distribution measurement

Master's Thesis

69 pages, 39 figures, 17 tables

Examiners: Professor Juhani Hyvärinen

Keywords:
Spray nozzle, spray droplet size distribution, shadowgraphy, Rosin-Rammler, Nukiyama-Tanasawa.

Spray nozzles are used in Nuclear Power Plants in order to condense and decrease the pressure of vapor in containment volume during Loss of Coolant Accidents and in pressurizer during its normal operation. Spray droplet size distribution and mean droplet diameters are needed for calculation of heat and mass transfer between the vapor and spray droplets. Computational Fluid Dynamic (CFD) codes can be used to simulate the spray flow and to test the performance of different spray nozzles.

The present Thesis deals with the spray droplet size distribution measurements of three pressure-swirl nozzles of different nominal capacities in the air atmosphere at room temperature by means of Shadowgraphy technique. The goal of this measurements is to get experimental data on droplet sizes in order to use it to validate spray droplet size distribution models built in CFD codes.

ACKNOWLEDGEMENTS

First of all, I want to thank my dear family: mother Natalia, father Valery and sister Anna for a constant support and love given to me all the time and making me feel close to home.

I wish to express my gratitude to professor Juhani Hyvärinen for a given opportunity to study in Lappeenranta University of Technology and for provided Master's Thesis topic.

I am very much obliged to my supervisor Lauri Pyy for his invaluable help in conduction of experiments, wise advices and regular guidance during processing of the data, and also for his unwavering patience.

I am very thankful to Nuclear Engineering Laboratory staff for mounting the experimental setup and their help during experiments.

And last but not least, special thanks go to my friend Eduard Musin for his constant support, endless sense of humor and our bracing gym sessions.

TABLE OF CONTENTS

ABSTRACT II

ACKNOWLEDGEMENTS III

LIST OF SYMBOLS AND ABBREVIATIONS 6

1 INTRODUCTION 8

1.1 Background of the Thesis 8

1.2 Goals and delimitations 8

1.3 Structure of the Thesis 9

2 BASICS OF LIQUID ATOMIZATION 12

2.2 Introduction 12

2.2 Breakup of liquid droplets 13

2.3 Breakup of liquid jets 14

2.4 Breakup of liquid sheets 16

3 SPRAY DROPLET SIZE DISTRIBUTIONS 18

3.1 Introduction 18

2.2 Graphical representation of droplet size distributions 18

3.3 Mathematical representation of droplet size distributions 20

3.3.1 Rosin-Rammler distribution 20

3.3.2 Nukiyama-Tanasawa distribution 20

3.4 Mean diameters 21

3.5 Representative diameters 22

4 CLASSIFICATION OF PRESSURE ATOMIZERS 23

4.1 Introduction 23

4.2 Plain orifice atomizer 23

4.3 Simplex atomizer 24

4.4 Dual orifice atomizer 25

4.5 Spill return atomizer 25

5 DROPLET SIZING 26

5.1 Introduction 26

5.2 FACTORS INFLUENCING DROPLET SIZE MEASUREMENT 26
5.2.1 Spatial and flux sampling 27
5.2.2 Sample size 28
5.2.4 Sampling location 28
6 ATOMIZERS IN NUCLEAR POWER PLANTS 30
6.1. THEORETICAL ASPECTS OF CONTAINMENT SPRAY SYSTEM NECESSITY 30
6.2 A BRIEF TECHNICAL DESCRIPTION OF CONTAINMENT SPRAY SYSTEM 31
6.3 THEORETICAL ASPECTS OF PRESSURIZER NECESSITY 33
6.4 PRESSURIZER OPERATING PRINCIPLES 34
7 DESCRIPTION OF EXPERIMENT 37
7.1 EXPERIMENTAL SETUP 37
7.2 INITIAL DATA FOR EXPERIMENT 39
7.3 SHADOWGRAPHY SYSTEM 39
7.4 BASICS OF THE SIZING ALGORITHM 40
8 RESULTS 43
8.1 TREATMENT OF EXPERIMENTAL DROPLET SIZE DATA 43
8.2 PROCESSING OF EXPERIMENTAL DROPLET SIZE DATA 50
8.3 RESULTS OF EXPERIMENT 54
DISCUSSION AND CONCLUSIONS 66
REFERENCES 68

LIST OF SYMBOLS AND ABBREVIATIONS

AMAD	Absolute Mean Average Deviation
CFD	Computational Fluid Dynamics
CSS	Containment Spray System
LOCA	Loss of Coolant Accident
LSS	Localization Safety System
LUT	Lappeenranta University of Technology
NPP	Nuclear Power Plant
PWR	Pressurized Water Reactor
RSS	Residual Sum of Squares
SAFIR	The Finnish Research Programme on Nuclear Power Plant Safety
VVER	Vodo-Vodyanoy Energeticheskiy Reaktor (Water Water Power Reactor)
ρ_L	liquid density
We	Weber number
ρ_A	surrounding medium density
U_R	relative velocity of droplet
σ	liquid surface tension
D	droplet diameter
C_D	drag coefficient of the droplet
Oh	Ohnesorge number
Re	Reynolds number
μ	liquid dynamic viscosity
d	initial diameter of undisturbed jet
λ_{opt}	wavelength of the fastest surface disturbances
λ	wavelength of initial disturbance
λ_{min}	minimum wavelength
N_i	bin heights of droplet number frequency distribution
ΔN_i	increment of number of droplets
ΔD_i	diameter increments in droplet size frequency distribution
N	total number of droplets
ΔQ_i	volume increments in droplet volume frequency distribution
Q_i	bin heights of droplet volume frequency distribution
Q	total volume of droplets

$F_V(D)$	droplet volume cumulative distribution
$f_V(D)$	droplet volume frequency distribution
$F_N(D)$	droplet number cumulative distribution
$f_N(D)$	droplet number frequency distribution
D_{10}	arithmetic mean diameter
D_{20}	surface mean diameter
D_{30}	volume mean diameter
D_{32}	Sauter mean diameter
$D_{0.1}$	droplet diameter such that 10% of the total liquid volume is in droplets of smaller diameter
$D_{0.5}$	mass median diameter
$D_{0.9}$	droplet diameter such that 90% of the total liquid volume is in droplets of smaller diameter
t_1	inlet reactor coolant temperature
Err	error
Γ	gamma function
D_{min}	diameter of the smallest droplet
dt	pulse delay time

1 INTRODUCTION

1.1 Background of the Thesis

One of the most important components of Pressurized Water Reactors (PWR) are Localization Safety Systems (LSS). These systems are the last barrier preventing release of fission products into the environment. Reliable operation of LSS ensures low probability of radioactive releases into the environment and provides economic attractiveness of Nuclear Power Plants (NPP). (Zorin, 2012, 533)

Containment Spray System (CSS) as a part of LSS is designed to reduce the temperature and pressure of gas-vapor medium that may enter the reactor building during depressurization of the various equipment (pipelines, steam generators, etc.). In order to ensure effective cooling, cold water is injected into gas-vapor environment in the form of droplets, which is done by nozzles located in the reactor building. As a result, vapor rapidly condenses on the droplet surfaces. The important function of CSS is collecting moving radioactive substances and binding them in the water; for that purpose, special reagents are added in the water. In existing systems, the necessary high pressure of the feed water is provided by an active system with special pumps. (Vorobiev et al., 2011, p. 1)

The main elements of CSS are nozzles that spray water in the form of droplets into the containment volume. The droplets have high surface to volume ratio which is favorable to ensure efficient heat and mass transfer between the water droplets and gas-vapor medium in the containment volume during Loss of Coolant Accidents (LOCA). During heat and mass transfer calculation it is necessary to know such spray characteristics as droplet size and velocity distributions, as well as arithmetic mean and Sauter mean diameters.

1.2 Goals and delimitations

Actual topic was chosen because Nuclear Engineering Laboratory of Lappeenranta University of Technology (LUT) was intended to perform spray droplet size analysis in order to get experimental data for validation of spray droplet distribution models integrated in CFD codes, which is a part of SAFIR, The Finnish Research Programme on Nuclear Power Plant Safety. For that purpose, LaVision's Shadowgraphy system was bought.

Droplet sizing analysis was never done before within the Laboratory. Therefore, the main reason for choosing this topic was to acquire pilot experience on how to install, calibrate and get the droplet size data using the equipment with such a relatively simple system as single spray nozzle in the air atmosphere with further perspective of studying more complex systems.

To achieve this, it is necessary to develop and mount a test bench with single spray nozzle with easy optical access to it, equipped with the necessary measuring instruments. Used measuring instruments should not introduce any distortions in the structure of the spray. In order to proceed with the problem of efficient heat transfer (outside the scope of this paper), it is also necessary to analyze the main factors influencing the spray droplet sizes in the experiments.

Measurements should be performed separately for several nozzles with different nominal capacities. The following parameters of the spray are to be determined and analyzed:

1. droplet size and droplet velocity distributions;
2. arithmetic mean and Sauter mean diameters.

It is also necessary to propose adequate mathematical description of measured experimental droplet size distributions of used nozzles, in order to be able to model them in CFD codes.

1.3 Structure of the Thesis

The Thesis is divided into two parts, theoretical and experimental part. In theoretical part basic mechanisms of droplet, jet and sheet disintegration are discussed in Chapter 2. Then graphical representation of spray droplet size distributions and theoretical Rosin-Rammler and Nukiyama-Tanasawa distributions are considered in Chapter 3, which is followed by discussion of various mean and representative diameters of spray droplet population. Classification of pressure atomizers, their different design solutions and operating principles are given in Chapter 4. Main factors influencing droplet size measurements are presented in Chapter 5. Application of atomizers in NPP are described in Chapter 6. The purpose of theoretical part is to give the reader a general view about subjects related to experimental part and to illustrate the complexity and importance of spray flows.

The experimental part starts with Chapter 7 where description of experimental setup and initial data for the experiment are given following by description of optical measuring system used to acquire the droplet data and sizing algorithm applied to this data. The detailed processing of the droplet data and obtained size and velocity distributions, mean and representative diameters can be found in Chapter 8. Conclusions on the Thesis and some recommendations to future researchers are provided in Discussion and Conclusions section of the paper.

Part I

Theory and Literature Study

2 BASICS OF LIQUID ATOMIZATION

2.2 Introduction

Atomization is a process of disintegration of bulk liquid into a dispersion of small droplets ranging in size from submicron to several hundred microns. Wide variety of devices has been developed which are generally termed as atomizers, sprayers or nozzles (Lefebvre, 2011, p. 1). The resultant suspension of droplets in a surrounding medium is disignated spray, mist or aerosol. Atomization of a liquid into separate droplets can be performed by a number of ways: aerodynamically, mechanically, ultrasonically, or electrostatically, etc. (Liu, 2000, p. 19). The most practical way to atomize a liquid is the pressure atomization where the pressure droplet in a nozzle is converted into kinetic energy of emanating liquid jet or sheet.

Atomization is affected by consolidating influence of surface tension and disruptive influence of internal and external forces. When consolidating surface tension dominates it pulls a liquid into the shape of sphere because it has the minimum surface energy. Liquid viscosity causes binding influence resisting any changes in system geometry. Oppositely, aerodynamic forces acting on the liquid surface cause disturbances and contribute to disintegration of the bulk liquid. Thus, breakup occurs when disruptive aerodynamic forces prevail consolidating surface tension forces. (Lefebvre, 1989, p. 27)

Atomization is considered to consist of two stages, first – primary atomization, in which a bulk liquid disintegrates in ligaments, second – secondary atomization, in which ligaments futher break up into smaller droplets. Processes occuring at both stages govern the shape, structure and penetration of the resulting spray along with characteristics of the droplet size and velocity distribution. Practically, these characteristics are affected by internal geometry and size of a nozzle, characteristics of surrounding medium in which the liquid is injected and the physical properties of the liquid itself. (Lefebvre & Ballal, 2010, p. 221 ; Lefebvre, 2011, p. 1)

At first, the different mechanisms of droplet breakup are considered because of their significance to both jet and sheet disintegration.

2.2 Breakup of liquid droplets

Atomization consists of a number of successive mechanisms, with breakup of larger droplets occurring on the final stages of spray development. Weber number, which is defined as a ratio of the breaking aerodynamic force, $0.5\rho_L U_R$, to the strengthening surface tension force, σ/D, is the important parameter of this process (Lefebvre, 1989, p. 31):

$$We = \frac{\rho_A U_R^2}{\sigma/D}, \tag{2.1}$$

where ρ_A – surrounding medium density, U_R – relative velocity of droplet, σ – surface tension, D – droplet diameter. Thus, the higher the value of Weber number, the more unstable the droplet. For any given liquid, the critical condition for droplet breakup is equality of aerodynamic drag and surface tension force (Lefebvre & Ballal, 2010, p. 222):

$$C_D \cdot \frac{\pi D^2}{4} 0.5\rho_A U_R^2 = \pi D^2 \cdot \sigma/D, \tag{2.2}$$

where C_D is the drag coefficient of the droplet. Rearranging of (2.2) yields (lbid.):

$$\left(\frac{\rho_A U_R^2 \cdot D}{\sigma}\right)_{crit} = 8/C_D, \tag{2.3}$$

where the left-hand side is the Weber number for critical condition. Experimental data for low-viscous liquids gives the average value of $8/C_D$ of *12*, thus (Ibid.):

$$We_{crit} = 12. \tag{2.4}$$

For subcritical Weber numbers surface tension force keeps the droplet stable, for supercritical Weber numbers external aerodynamic force prevails and causes breakups.

In order to take into account liquid viscosity, Ohnesorge number is introduced (Lefebvre & Ballal, 2010, p. 223):

$$Oh = \frac{We^{0.5}}{\mathrm{Re}}, \tag{2.5}$$

where $We = \rho_L U_R^2 D/\sigma$ and $\mathrm{Re} = \rho_L U_R D/\mu_L$, where ρ_L – liquid density, μ – liquid dynamic viscosity. Substituting *We* and *Re* to (1.5) gives (Ibid.):

$$Oh = \frac{\mu_L}{(\rho_L \sigma D)^{0.5}}. \tag{2.6}$$

Liquid viscosity can be considered by introducing extra term in critical Weber number:

$$We_{crit} = We_{crit,0} + 14Oh^{1.6}, \tag{2.7}$$

where $We_{crit,0}$ - critical Weber number for zero viscosity. (Ibid.)

2.3 Breakup of liquid jets

The classical mechanism of jet and sheet breakup is based on the method of small disturbances which are created either within or on the jet surface. These disturbances induce the formation of waves which propagate and cause breakup of liquid jet and generation of droplets (Lefebvre & Ballal, 2010, p. 223). These disturbances may be in the form of surface displacement, fluctuations of pressure and velocity as well as physical properties of liquid (Ashgriz, 2011, p. 3).

Rayleigh studied the breakup of liquid jets using the assumption of inviscid liquid. He postulated that a laminar liquid jet becomes unstable only when the wavelength of the fastest surface disturbances, λ_{opt}, reaches $4.51d$, where d is initial diameter of undisturbed jet (Lefebvre, 1989, p. 39). The process of jet breakup according to Rayleigh's theory is illustrated in Figure 2.1.

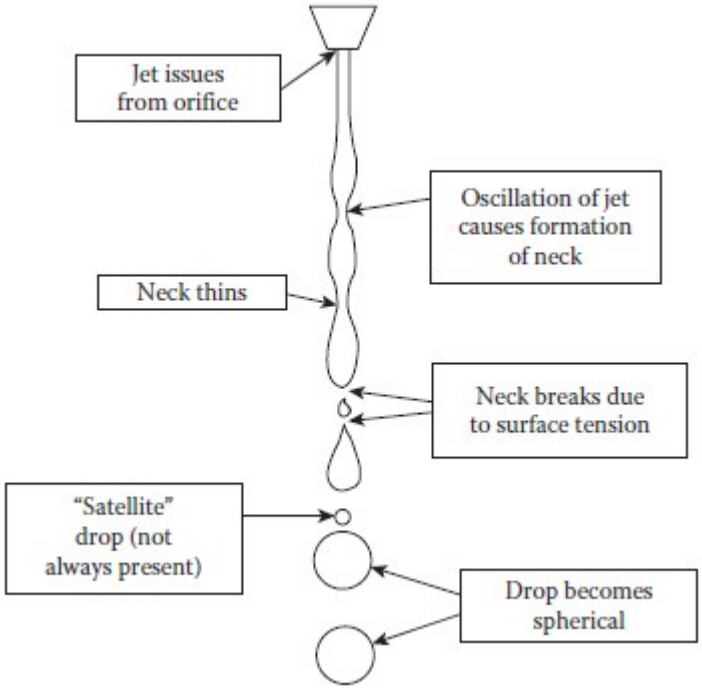

Figure 2.1. Breakup of a round jet at low velocity (Lefebvre & Ballal, 2010, p. 224)

Further downstream, only the fastest class of disturbances propagates and governs the process of jet disintegration (Liu, 2000, p. 127). After breakup, the cylindrical jet of length $4.51d$ turns to spherical droplet, so that (Lefebvre & Ballal, 2010, pp. 224, 225):

$$4.51d \cdot \frac{\pi d^2}{4} = \frac{\pi D^3}{6}, \tag{2.8}$$

hence D, the diameter of generated droplet:

$$D = 1.89d\,. \tag{2.9}$$

Later Weber extended Rayleigh's theory of jet breakup at low jet velocities and considered liquid viscosity. According to his assumptions, any disturbance induces axisymmetrical oscillations of the jet, as illustrated in Figure 2.2.

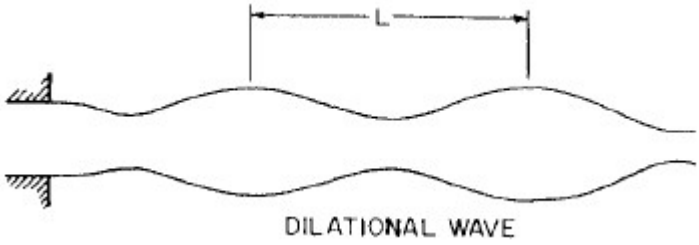

Figure 2.2. Jet with axisymmetrical disturbance (Lefebvre, 1989, p. 40).

In doing so, if the wavelength of initial disturbance, λ, is less than λ_{min}, the surface tension force dumps out the disturbance, otherwise the surface tension force amplifies the disturbance. In latter case jet eventually disintegrates. The minimum wavelength is equal to the jet circumference $\lambda_{min}=\pi d$ for both inviscid and viscous liquids, which is consistent with Rayleigh's theory. However, there is a particular wavelength, λ_{opt}, at which the liquid disintegration is the most favorable, following (Liu, 2000, p. 135):

$$\lambda_{opt} = \sqrt{2}\pi d = 4.44d \qquad \text{- for inviscid liquids} \tag{2.10}$$

$$\lambda_{opt} = \sqrt{2}\pi d\left(1 + 3Oh\right)^{0.5} \qquad \text{- for viscous liquids} \tag{2.11}$$

Thus, accounting for liquid viscosity introduces Ohnesorge number, which enlarges the optimum wavelength for jet breakup and thereby increases the size of formed droplets (Lefebvre & Ballal, 2010, p. 225).

Weber also studied the effect of increasing jet velocity on droplet size. He found that increasing the relative velocity between the liquid jet and the surrounding medium reduces the optimum wavelength for jet breakup, resulting in a smaller droplet size. At very high jet velocities, atomization occurs rapidly and finishes within a short distance from the nozzle orifice. (Lefebvre & Ballal, 2010, pp. 225, 226).

2.4 Breakup of liquid sheets

Most atomizers emit the liquid in the form of flat, fan or conical sheet. Subsequent development of liquid sheet depends on liquid velocity and physical properties of both the liquid and surrounding medium. Sheet breakup is more complex than that of jet breakup because three-dimensional flow takes place (Nasr, et al., 2002, p. 13). The minimum sheet velocity is required in order to overcome the consolidating surface tension force. Increasing the liquid velocity expands and lengthens the sheet until the formation of leading edge where balance between surface tension and aerodynamical forces is achieved. Droplet size distribution is determined by the orderliness of atomization and the uniformness of generated liquid threads and ligaments (Lefebvre, 1989, p. 60).

According to Fraser et al., there are three modes of sheet disintegration as illustrated in Figure 2.3. (Liu, 2000, p. 151).

(a)

(b)

(c)

Figure 2.3. Modes of liquid sheet/film disintegration: (a) – rim disintegration; (b) – wave disintegration; (c) – perforated-sheet disintegration (Liu, 2000, p. 152).

In the rim mode, the free edge of a liquid is contracted into a thick rim by surface tension forces (Figure 2.3, a), which then disintegrates by the same mechanism as a liquid jet. Resulting droplets continue moving in the initial direction remaining attached to the receding surface by threads that thin and rapidly break into rows of small droplets. Consequently, large droplets and many smaller satellite droplets are generated (Lefebvre, 1989, p. 60). This breakup mode is most typical for liquids with high viscosity and high surface tension, such as liquid metals (Liu, 2000, p. 151).

In the wave mode, oscillations are set on a liquid surface as a result of interaction with a surrounding medium. When their amplitude increases to a critical value, the parts of the sheet, ending at a half or full wavelength of the oscillation, are ripped away and rapidly contract into unstable ligaments cased by the action of surface tension. Subsequently, these ligaments break up into droplets by aerodynamical or turbulent forces before a regular network of threads can be formed (Lefebvre, 1989, p. 60). Wave disintegration is highly irregular resulting in significantly wide droplet size range (Liu, 2000, p. 151).

In the perforated-sheet mode holes appear in the liquid sheet, the liquid that was originally inside the holes, surrounds them forming the rims. These rims quickly increase in size until the adjacent rims merge producing ligaments and threads of irregular shape that eventually disintegrate into droplets of various sizes. Perforations on a liquid sheet have a similar evolution history since they occur at the same distance from the nozzle, thus producing threads of fairly regular size resulting in uniform droplet sizes. (Lefebvre, 1989, p. 60)

Atomizers discharging the liquid in the form of sheet can operate in each of these three modes. Some atomizers can exhibit two of the modes simultaneously, and their relative importance affect both the droplet size distribution and mean droplet size. Liquid sheets with high viscosity and high surface tension are most resistant to disruption, while effect of liquid density on sheet disintegration is very small. (Liu, 2000, pp. 153, 154)

3 SPRAY DROPLET SIZE DISTRIBUTIONS

3.1 Introduction

The threads and ligaments and subsequent droplets formed during atomization vary widely in size due to randomness and chaoticness of the atomization process. Such heterogeneous structure of sprays leads to spectrum of droplet sizes usually varying from a few microns up to several millimeters. Many applications require accurate control of droplet size distribution and mean droplet size to attain the necessary heat and mass transfer rates, or to satisfy specific requirements of an application. Thus, it is very important to determine these parameters. Droplet size distribution can be presented both graphically and mathematically. (Lefebvre, 1989, p. 79 ; Liu, 2000, p. 240)

2.2 Graphical representation of droplet size distributions

A simple and visual method to illustrate the droplet size distribution is to plot histogram where the bin height in size range i, N_i, is expressed as follows:

$$N_i = \frac{\Delta N_i}{N \cdot \Delta D_i}, \tag{3.1}$$

where ΔN_i – number of droplets within the limits D_i-$\Delta D_i/2$ and D_i+$\Delta D_i/2$, ΔD_i – diameter increment in size range i, N – total number of droplets, following:

$$N = \sum_i \Delta N_i \, . \tag{3.2}$$

Histogram which ordinate values are expressed in a form (3.1) is called droplet number frequency distribution. (Lefebvre, 1989, p. 80 ; Ashgriz, 2011, p. 480)

If, instead of plotting the number of droplets, the volume/mass of droplets is plotted as a histogram of droplet size, the resulting distribution is skewed to the right, as illustrated in Figure 3.1, due to the weighting effect of the larger droplets. (Lefebvre, 1989, p. 80)

Volume increments, ΔQ_i, can be recalculated from the number increments, ΔN_i, by the following formula:

$$\Delta Q_i = \Delta N_i \frac{\pi}{6} \left[0.5\left(D_i + D_{i+1}\right)\right]^3 . \tag{3.3}$$

Bin heights of droplet volume frequency distribution, Q_i, are obtained similarly to (3.1):

$$Q_i = \frac{\Delta Q_i}{Q \cdot \Delta D_i}, \tag{3.4}$$

where Q – total volume of droplets, following:

$$Q = \sum_{i=1}^{N} \Delta Q_i \,. \tag{3.5}$$

By expressing ordinate values of histograms in the forms (3.1) and (3.4) their unit is length^{-1} and the area under the histograms is equal to *1.0.* (Lefebvre, 1989, p. 80).

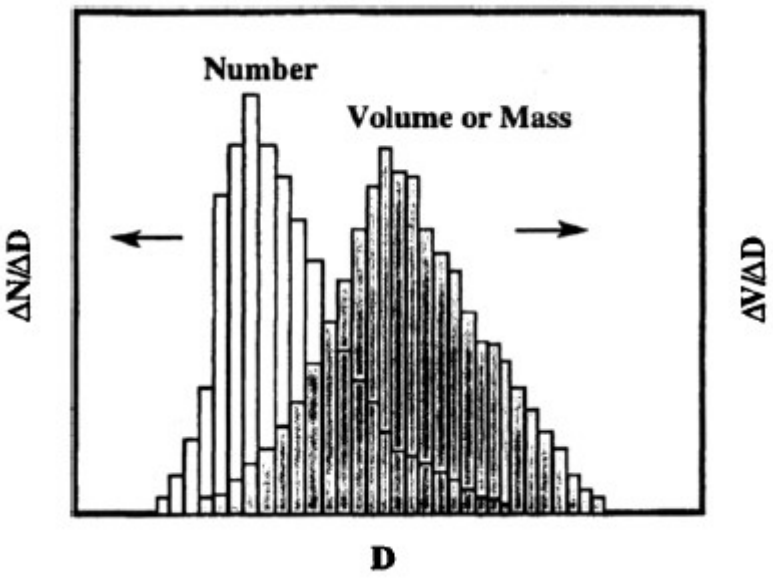

Figure 3.1. Typical droplet size distributions based on number and volume of droplets. (Lefebvre & Ballal, 2010, p. 241)

As *ΔD* is made smaller in (3.1) and (3.4) the histogram turns to a continuous frequency distribution curve that is used to describe large samples of droplet size data.

Droplet size distribution can also be expressed in a form of cumulative distribution which is an integral plot of the frecuency distribution. It illustrates the percentage of the total number of droplets, surface area or volume of a spray contained in droplets below a given size. (Liu, 2000, p. 240).

3.3 Mathematical representation of droplet size distributions

At the moment, no fundamental mechanism or model on which to build a theory of droplet size distributions is known. Therefore, proposed mathematical functions are based on probability or purely empirical considerations. A significant advantage of mathematical representation is that used functions describe the entire droplet size distribution while featured by parameters calculated from limited samples of droplet size measurements. Generally used functions include normal, log-normal, upper-limit, Rosin-Rammler and Nukiyama-Tanasawa distributions, with two last ones being most commonly used. It is generally accepted that no single distribution function can represent all droplet size data with the same quality. Usually it is recommended to try several distribution functions to find the best fit to the relevant experimental data (Sirignano, 2010, p. 5 ; Lefebvre & Ballal, 2010)

3.3.1 Rosin-Rammler distribution

Rosin-Rammler droplet size distribution was originally developed to characterize the droplet volume cumulative distribution of coal particles after grinding and probably the most widely used at present:

$$F_V(D) = 1 - \exp\left[-\left(\frac{D}{m}\right)^n\right], \tag{3.6}$$

where $F_V(D)$ – fraction of the total liquid volume contained in the droplets of diameter less than D, m – droplet diameter such that 63.2% of the total liquid volume is in the droplets of smaller diameter, n – constant to be determined to fit the relevant experimental data. The value of n shows the spread of droplet sizes. The higher the value of n, the more uniform the spray. For most practical sprays the value of n ranges between *1.5* and *4*. If n is equal to infinity, all the droplets in the spray are the same size. Since the distribution function has infinite range of droplet sizes it allows extrapolation of data down to the range of very small diameters where measurements are most difficult and least accurate. (Ashgriz, 2011, p. 483 ; Lefebvre, 1989, p. 87)

3.3.2 Nukiyama-Tanasawa distribution

Nukiyama-Tanasawa droplet size distribution was originally developed to characterize the droplet number frequency distribution of sprays of pneumatic nozzles:

$$f_N(D) = \frac{dN}{dD} = aD^p \exp\left(-bD^n\right), \tag{3.7}$$

where a, *b*, *p, n* – constants to be determined to fit the relevant experimental data. The distribution height is adjusted by the value of *a*, while distribution width and location of the mean are set by *b*, *p,* and *n*. Results are meaningful if only *p>1* and *n>0* or *p<-4* and *n<0*. Equation (3.7) contains four independent constants which are difficult to adjust simultaneously. Thus, in practice it is used in simplified or modified forms discussed later in Chapter 8.2. (Ashgriz, 2011, p. 483 ; Lefebvre, 1989, p. 86).

3.4 Mean diameters

In many mass transfer and flow processes the whole droplet size distribution can be conveniently represented by mean droplet diameters. The concept of mean diameter was generalized and its notation standardized by Mugele and Evans. A general form of mean droplet diameter is written as:

$$D_{ab} = \left[\frac{\int_{D_{\min}}^{D_{\max}} D^a f_N(D) dD}{\int_{D_{\min}}^{D_{\max}} D^b f_N(D) dD} \right]^{\frac{1}{a-b}}, \tag{3.8}$$

where $f_N(D)$ – droplet number frequency distribution, *a* and *b* – positive integers taking the values according to the application considered. (Lefebvre, 1989, p. 90)

Practically, it is easier to deal with discrete form of Eq. (3.8), following:

$$D_{ab} = \left[\frac{\sum_{i=1}^{N} \Delta N_i D_i^{\,a}}{\sum_{i=1}^{N} \Delta N_i D_i^{\,b}} \right]^{\frac{1}{a-b}}, \tag{3.9}$$

where *i* – size range considered, ΔN_i – number of droplets in size range *i*, D_i – middle diameter of size range *i.* (Ashgriz, 2011, p. 481)

Most commonly used mean diameters include: arithmetic mean diameter (D_{10}), surface mean diameter (D_{20}), volume mean diameter (D_{30}), Sauter mean diameter (D_{32}). Thus, for example, D_{32} is the diameter of the droplet whose ration of volume to surface area is the same as that of the whole spray. (Liu, 2000, pp. 248, 249)

3.5 Representative diameters

The droplet size distribution can usually be characterized as a function of two parameters: the mean or representative diameter, and the measure of the spread of droplet sizes. (Lefebvre, 1989, p. 91)

There are many representative diameters, which are related to each other via some formulas and thereby can be used to define the droplet size distribution interchangeably. The most commonly used representative diameters are: $D_{0.1}$, $D_{0.5}$ (mass median diameter, *MMD*), $D_{0.632}$ (*m* in Eq. (3.6)), and $D_{0.9}$ - droplet diameter such that 10%, 50%, 63.2%, and 90% (correspondingly) of the total liquid volume is in droplets of smaller diameter. (Lefebvre & Ballal, 2010, p. 234)

4 CLASSIFICATION OF PRESSURE ATOMIZERS

4.1 Introduction

The main function of atomizers is to transform a bulk liquid into suspension of fine droplets. Atomizers can be categorized in relation to the way used to produce the instability of a liquid. For instance, pressure is used in pressure atomizers, gas/fluid in twin-fluid atomizers, centrifugal force in rotary atomizers, and vibration in ultrasonic or acoustic atomizers. What is available as a source of energy often defines the choice of atomizer. (Liu, 2000, p. 20 ; Nasr, et al., 2002, p. 17)

In pressure atomizers, a liquid achieves a high velocity relative to surrounding medium by conversion of pressure into kinetic energy. In many application areas pressure atomizers are ones of the most commonly used. They include plain orifice, simplex, dual orifice and spill return atomizers which are considered below. (Lefebvre & Ballal, 2010, p. 237)

4.2 Plain orifice atomizer

In plain-orifice atomizer liquid passes through a small round hole which is most efficient for low-viscosity liquids (see Figure 4.1, a). At low discharge velocity, the liquid leaves the orifice as a thin distorted pencil, but as soon as injection pressure differential exceeds about 150 kPa, liquid ejects as a high-velocity jet and rapidly disintegrates into droplets. Break-up of the jet enhances increasing in injection pressure, which increases both the aerodynamic forces caused by the surrounding medium and the turbulence in the liquid jet. The angle of the spray cone formed by a plain-orifice atomizer varies typically from 5° to 15°. (Lefebvre & Ballal, 2010, p. 238 ; Liu, 2000, p. 27)

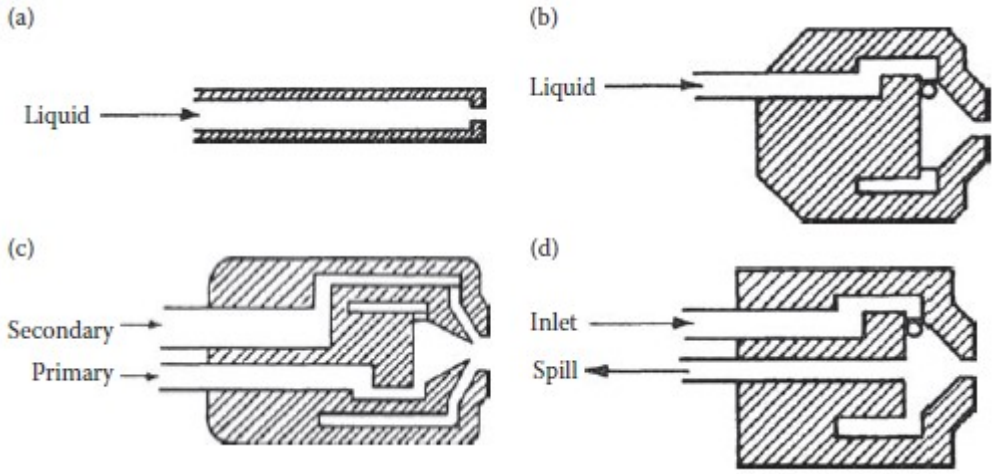

Figure 4.1. Pressure-swirl atomizers: (a) plain orifice; (b) simplex; (c) dual orifice; (d) spill return (Lefebvre & Ballal, 2010, p. 238).

4.3 Simplex atomizer

Narrow spray cone angles which are inherent to plain-orifice atomizers are unsuitable for most practical applications. Pressure-swirl atomizers produce much wider cone angles which is achieved by imparting a swirling motion to the liquid. The spray cone angles range from 30° to almost 180°, which depends on the ratio of the radial and axial velocity components at the nozzle exit. (Lefebvre & Ballal, 2010, pp. 238, 239 ; Liu, 2000, p. 29)

The simplex atomizer is the simplest form of pressure-swirl atomizer (see Figure 4.1, b). Simplex atomizer houses conical swirl chamber with a small orifice at the vertex. Liquid is supplied into a swirl chamber through tangential ports that give it angular velocity, which creates an air-cored vortex. The rotating liquid flows through the nozzle orifice under both axial and radial forces and spreads out in a hollow cone pattern. The droplet size depends on liquid pressure and dimensions of the swirl chamber. The smaller the swirl chamber, the finer the generated droplets. (Ibid.)

Other designs of simplex atomizer provide solid cone pattern, but their main drawback is relatively coarse atomization, the droplets at the center of the spray are larger than those near periphery. (Lefebvre, 1989, p. 112)

A flow rate of simplex atomizes varies as the square root of the injection pressure differential, which is their major drawback. For example, low-viscosity liquids can be

atomized at the lowest injection pressure of about 0.1 MPa. Thus, increasing the flow rate to 20 times the minimum value requires an injection pressure of 40 MPa, which is beyond the capability of most pumps. (Lefebvre & Ballal, 2010, p. 239)

4.4 Dual orifice atomizer

Dual orifice atomizer solves the major drawback of simplex atomizer. Here the ratios of maximum to minimum flow rate of 20 and higher can be achieved with injection pressures not exceeding 7 MPa. A dual orifice atomizer consists of two concentrically fitted simplex nozzles (see Figure 4.1, c). For low flow rates, all the liquid flows through the primary nozzle providing high atomization quality because a relatively high liquid pressure is needed to force the liquid through the small ports in the primary swirl chamber. Increasing the liquid flow rate, a liquid pressure reaches the point when a valve opens admitting the liquid to the secondary nozzle. In the beginning, atomization quality is poor because the liquid pressure in the secondary nozzle is low. Further increasing the flow rate, this pressure raises which improves atomization quality. (Lefebvre & Ballal, 2010, p. 239)

4.5 Spill return atomizer

This is a simplex atomizer featuring a passage on the rear wall of the swirl chamber through which liquid can be diverted away from the nozzle (see Figure 4.1, d). The liquid is always fed to the swirl chamber at the maximum pressure and flow rate. During the operation of the nozzle at its maximum capacity, the spill line valve is fully closed and all the liquid exits the nozzle orifice and spreads out as a well-atomized spray. When the valve is open, liquid is spilled away from the swirl chamber so that less of it passes through the nozzle orifice. Thus, constant use of a relatively high pressure provides adequate swirl needed for efficient atomization even at extremely low flow rates. (Lefebvre, 1989, p. 122)

Another attractive feature of the spill return atomizer is an absence of moving parts resulting in high resistance to blockage by contaminants in the liquid. The principal drawbacks are high pump power requirements and a wide variation in spray cone angle with change in liquid flow rate. (Ibid.)

5 DROPLET SIZING

5.1 Introduction

Measurements of spray droplet properties are needed in many branches of scientific research and engineering applications. An accurate and detailed measurements of droplets in a spray is essential, for example, for understanding of spray processes and validating of spray modeling. Many measuring techniques have been used meeting some challenges because of number of features inherent to a spray. These include very large number of droplets in a spray, the high and varying velocity the droplets, the wide range of droplet sizes presented in most practical sprays (the ratio of the largest to the smallest droplet is often greater than 100), and also the changes in droplet sizes with time as a result of evaporation and coalescence. (Liu, 2000, p. 397 ; Lefebvre, 1989, p. 367)

Ideal droplet sizing technique should feature the following characteristics:

1. Cause no disturbance to the atomization process or spray pattern;
2. Cover a wide range of droplet sizes;
3. Have the ability to measure both spatial and temporal distributions;
4. Where appropriate, provide large representative sample sizes;
5. Tolerate wide changes in liquid and surrounding medium properties;
6. Provide rapid means of sampling and counting.

No single technique has all mentioned characteristics; thus, the capabilities and limitations of the various available measuring techniques must be recognized. (Lefebvre, 1989, pp. 367, 368)

5.2 Factors influencing droplet size measurement

All measuring techniques are subject to errors and ambiguities dependent on the method applied. However, there are several sources of error inherent to almost all techniques, which are discussed below. (Lefebvre, 1989, p. 368)

5.2.1 Spatial and flux sampling

There are two types of sampling techniques to measure droplet size distribution. Spatial technique implies instantaneous sampling of collection of droplets contained in a given volume (see Figure 5.1). Flux (also known as temporal) technique samples individual droplets passing through a fixed cross-sectional area during a specific time interval (see Figure 5.2). If all droplets in a spray move at the same velocity, the results provided by both techniques are identical. If not, temporal droplet size distribution can be obtained from spatial one by multiplying the number of droplets in each size class by the average velocity of droplets in that size class. (Lefebvre, 1989, pp. 369, 370 ; Schick, 2008, pp. 6, 7)

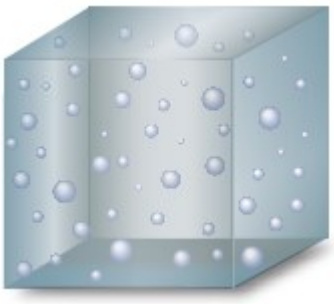

Figure 5.1. Sampling volume in spatial technique. (Schick, 2008, p. 6)

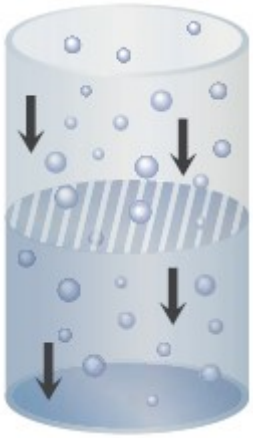

Figure 5.2. Sampling cross-section in flux technique. (Ibid.)

The sampling technique is important in understanding and comparing the droplet size data obtained from different sizing methods. In pressure atomizers, smaller droplets decelerate more rapidly than bigger droplets thereby creating high concentration of smaller droplets near the nozzle orifice. Thus, spatial sampling in this region gives the smaller values for

mean diameters than those obtained using flux sampling. Further downstream, where all the droplets move at approximately equal velocities, both techniques provide close results. (Ibid.)

5.2.2 Sample size

Before gathering of droplet data, it is beneficial to know the necessary and sufficient sample size. An undersized sample would not represent the actual population, whereas an oversized sample involves more resources such as unnecessary usage of equipment, extra time for analyzing and processing, and extra costs for larger data storages. (Pimentel, 2006, p. 81)

The necessary and sufficient sample size depends on the dispersion of droplet diameters in a spray, the acceptable accuracy and the level of confidence desired to achieve the above parameters. The literature review shows that there is lack of information on such sample sizes, especially that considering the dispersion of droplet diameters in a spray. The accuracy of the mean diameter obtained for various sample sizes for 95% confidence interval is presented in Table 5.1. (Pimentel, 2006, p. 81 ; Lefebvre, 1989, p. 370)

Table 5.1. Influence of sample size on accuracy of measurement of droplet mean diameter. (Lefebvre, 1989, p. 370)

Number of droplets in sample	Accuracy, %
500	±17
1500	±10
5500	±5
35000	±2

As mention above, Table 5.1 neither contains information on the dispersion of the droplet diameters in a spray, although it affects the sample size significantly. (Ibid.)

5.2.4 Sampling location

Some measuring techniques enable sampling of sufficiently representative volumes of the entire spray cone, while the others can extract the data only from the very limited volumes. The latter techniques require much longer time to obtain enough data to characterize the entire spray. Most of the pressure-swirl atomizers generate heterogeneous distribution of

droplets along both axes of the spray cone. The larger droplets are more concentrated at the periphery of the spray cone and further downstream of the nozzle because of their higher inertia. Thus, the local measurements of such sprays give misleading information about their droplet size distribution. (Lefebvre, 1989, p. 372)

The mean droplet size and droplet size distribution change with axial direction because of the development of atomization process in a spray. Ideally, measurements should be carried out in a plane near the nozzle orifice where atomization process is just completed. Unfortunately, in practice its location is difficult to define because it depends on nozzle design, injection pressure, liquid flow rate, and surrounding ambient properties. (Ibid.)

6 ATOMIZERS IN NUCLEAR POWER PLANTS

In this chapter, theoretical aspects and basic operating principles of NPP systems having the spray nozzles as one of the main element are discussed. These systems are exemplarily considered in terms of VVER-1000/V-320 rector plant.

6.1. Theoretical aspects of containment spray system necessity

Loss of Coolant Accident caused by damage to the equipment and piping of the primary circuit is one of the most dangerous. During the accident, the medium ejecting from the ruptured pipe (with inner diameter of 850 mm) under extremely high pressure and temperature may cause release of radioactive substances into the interior of technological facilities. In order to keep it within technological boundaries, containment is used. (Technological systems of reactor plant. Part 1, 1999, p. 56)

Containment is a cylinder with inner diameter of 45 meters, combined with a flat bottom and domed top. Dome elevation - 66.55 m (see Figure 6.1). Thickness of cylindrical part of the wall is 1.2 m, thickness of the dome is 1.1 m. Containment volume is 67000 m^3. According to the project it is designed to withstand internal pressures up to 4.9 bar, arising from primary circuit rupture and complete escape of coolant under containment. Permissible value of leakage is 0.3% of the overall containment volume per day. (Zorin, 2012, p. 533)

In case of LOCA it is desirable to decrease the pressure in the containment to reduce the leakage of radioactive substances from containment building. In order to mitigate the effects of large releases of vapor and reduce pressure in the containment during LOCA, a special safety system called “Containment Spray System” is provided. (Zorin, 2012, p. 536)

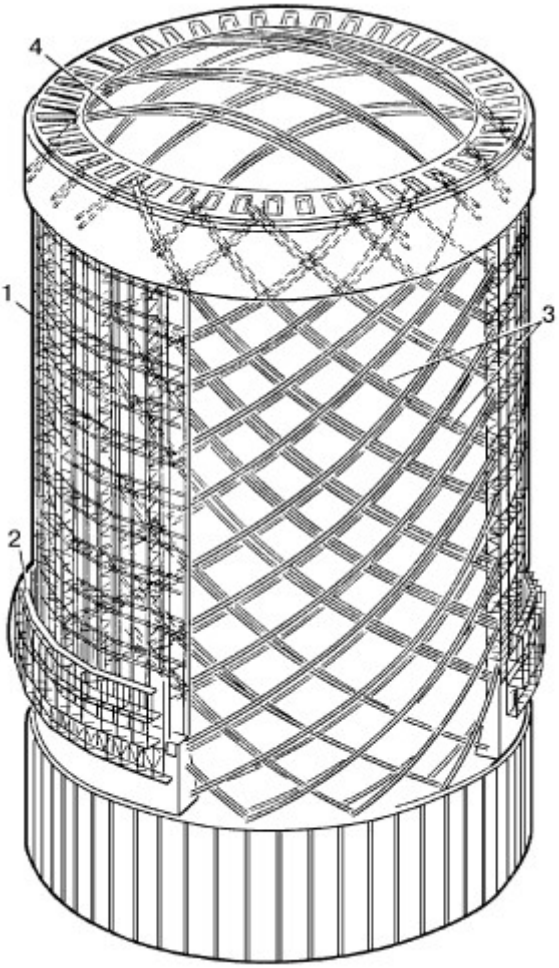

Figure 6.1. Structure of containment of VVER-1000/V-320 project. (Technological systems of reactor plant. Part 1, 1999, p. 56)
1 – reinforcement cage; 2 – formwork; 3 – polyethylene channeling of cylindrical part; 4 – polyethylene channeling of domed part.

6.2 A brief technical description of Containment Spray System

Equipment of the CSS is marked with Latin letters TQ as all other safety systems, the first channel of the CSS is denoted as TQ11, the second channel - TQ21, the third channel - TQ31. (Technological systems of reactor plant. Part 1, 1999, p. 57)

Containment Spray System TQ11-31 is designed for:

1. reduction of pressure within localization buildings during depressurization of one or two circuits;
2. binding of radioactive isotopes of iodine;

3. emergency filling of spent fuel pool in the modes when the access of normal cooling water is blocked. (Ibid.)

The composition of each subsystem includes (see Figure 6.2):

1. sprinkler pump TQ11D01;
2. tank with sprinkler solution TQ11B01;
3. water-jet pump TQ11D02;
4. spray nozzles (20 in each channel);
5. piping, valves, instrumentation. (Ibid.)

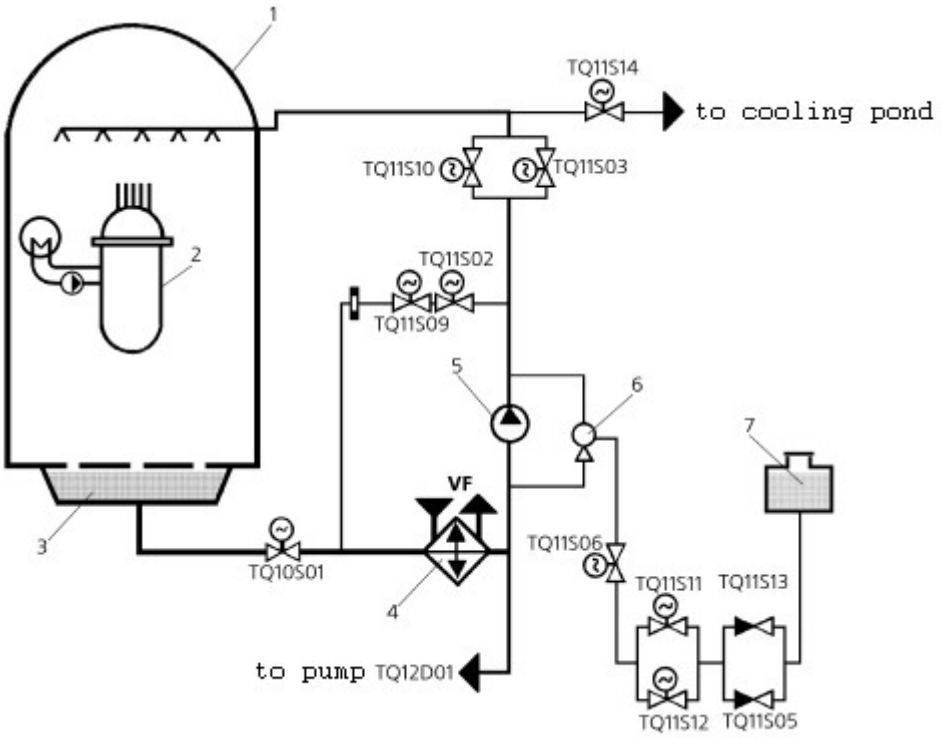

Figure 6.2. Simplified scheme of CSS (TQ11 channel). (Ibid.)
1 – containment; 2 – primary coolant circuit; 3 – tank GA-201; 4 – heat exchanger TQ10W01; 5 – sprinkler pump TQ11D01; 6 – water-jet pump TQ11D02; 7 – tank with sprinkler solution TQ11B01.

The main water channels end up with three independent rings under the containment dome at elevations of 62-64 m, where the nozzles are arranged so as to provide the most uniform irrigation of the entire volume of the containment. Pressure manifold of each CSS subsystem is equipped with 20 spray nozzles providing uniform atomization of the sprinkle

solution over the large area. The main working parameters of the nozzles are listed in Table 6.1. (Ibid.)

Table 6.1. Main working parameters of the nozzles. (Spray nozzles, 2016)

Parameter	**Value**
Volume flow rate, m^3/h	30
Pressure drop, MPa	0.098
Design pressure, MPa	1.13
Design temperature, °C	150
Working temperature, °C	≤ 90
Spray cone angle	≥ 75°
Arithmetic mean droplet diameter, mm	0.8

The system activates automatically and injects the borated water under containment when pressure exceeds the design limit of 4.9 bar. Borated water is sprinkled into containment volume by spray nozzles, decreasing the pressure and temperature due to condensation of vapor, then it flows down to the tank of emergency reserve of boron (GA-201), and being cooled in the emergency and planned cooling heat exchanger TQ10W01 flows to the suction pipe of sprinkler pump. (Ibid.)

6.3 Theoretical aspects of pressurizer necessity

The water in the primary circuit has a relatively large coefficient of thermal expansion and low compressibility, which leads to unacceptably large pressure changes with changing temperature of the primary circuit (even under normal transient conditions). For example, at a pressure of 9.8 MPa and the temperature change from 250 to 300°C, a specific volume of water increases by 11%. When heating primary circuit of VVER-1000 from cold ($t_1 < 70°C$) to hot ($t_1 = 280°C$) state the coolant density reduces by 30%. This requires organization of a special compensating volume in the primary circuit. (Main equipment of reactor plant, 1999, p. 77 ; Zorin, 2012, p. 466)

For the above reasons, PWRs feature pressure (volume) compensation system called “pressurizer” with damping element in the form of a vapor cushion. Pressurizer is a component of the reactor plant and is designed to create and maintain the pressure in the primary circuit in stationary mode, to limit pressure deviation in the transitional and emergency modes (see Figure 6.3). (Ibid.)

6.4 Pressurizer operating principles

The pressure inside pressurizer is created by a vapor cushion formed in the upper part of the pressurizer by water boiling. Boiling is achieved by heating by tubular heating elements located below the water level in the lower part of pressurizer. (Main equipment of reactor plant, 1999, pp. 81, 82 ; Zorin, 2012, p. 469)

When the average temperature of the coolant changes in the transients associated with equipment malfunctioning and load change, some of the coolant flows via connecting pipeline (with inner diameter of 350 mm) from pressurizer to circuit or vice versa. In doing so limiting of the pressure deviations from the nominal value is achieved by compressing or expanding the vapor cushion in pressurizer. Pressure variation range is 11.8-17.7 MPa. (Main equipment of reactor plant, 1999, pp. 81, 82 ; Zorin, 2012, p. 466)

The water volume is also involved in the pressure balancing process: water evaporates generating more vapor keeping up the pressure; vapor condenses on the surface of the water limiting the pressure rise. Under the large pressure increase, coolant from the cold leg of the first loop of primary circuit is fed into pressurizer by the nozzles located in its upper part to condense the vapor in the vapor cushion. Depending on the transient, supply of cold coolant slows down or completely stops the pressure rise in the primary circuit. (Main equipment of reactor plant, 1999, p. 82 ; Zorin, 2012, p. 470)

The nozzles are meant for spraying the water over the volume of steam for its condensation. Manifold distributing the water has four nozzles. Manifold is attached to the channel bars, which are welded to the upper bottom of the pressurizer. The nozzles are mounted on the threaded branch pipes of the distributing manifold. (Main equipment of reactor plant, 1999, p. 83)

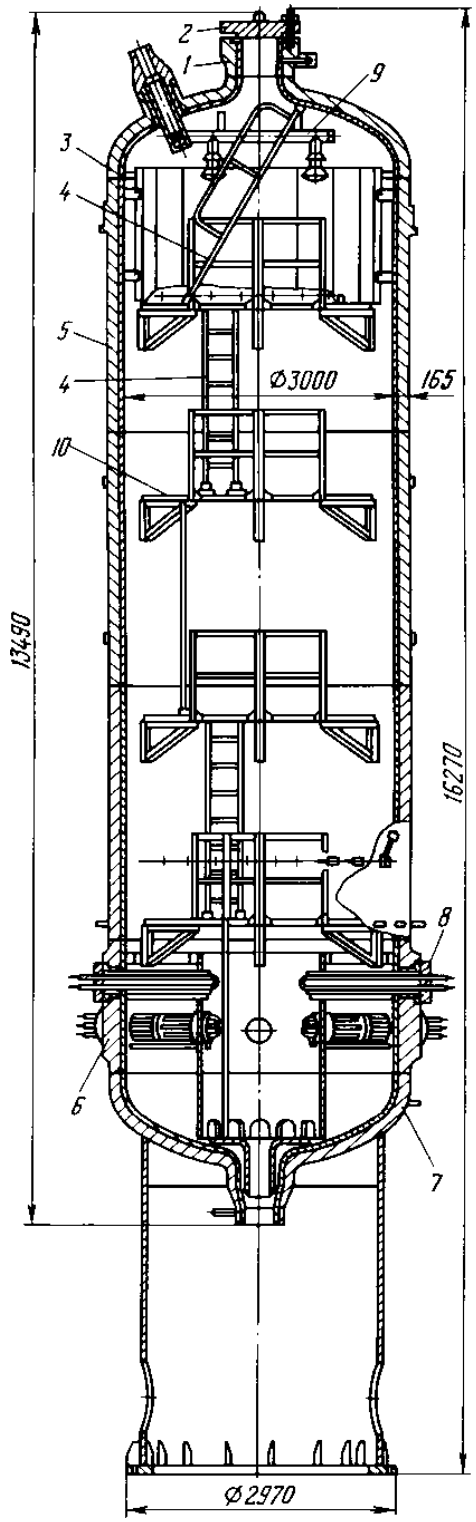

Figure 6.3. Pressurizer. (Ibid)

1 – manhole; 2 – lid; 3 – upper bottom; 4 – ladder; 5 – shell; 6 – sidewall of block of tubular heating elements; 7 – bottom; 8 – block of tubular heating elements; 9 – distributing manifold; 10 – maintenance platform.

Part II

Experiments and Analysis

7 DESCRIPTION OF EXPERIMENT

7.1 Experimental setup

The experiments were carried out in Nuclear Engineering Laboratory of LUT. The experimental setup is composed of a water pipe supplying, for these experiments, three different spray nozzles that are removably attachable to the end of the pipe (see Figure 7.1). Sprays are investigated at ambient room temperature, atmospheric pressure and at injection water pressure measured by pressure gauge installed within water supply pipe. The water temperature is measured with a thermal element from the line connected to the spray nozzle. The sprayed water is collected with a drain hole on the floor. All setup is installed on the stacker truck, spray nozzle itself is fastened to its movable part so that axial position of the nozzle head can be adjusted by changing the height of this part.

Figure 7.1. Experimental setup.

Experiments were conducted with three different pressure-swirl full cone nozzles from Spraying Systems Co. Their characteristics at the nominal pressure of 1.5 bar are listed in Table 7.1.

Table 7.1. Characteristics of spray nozzles used in experiments (Industrial hydraulic spray products. Catalog 75A-M HYD, 2015, p. B7).

	Inlet connection, mm	**Orifice diameter, mm**	**Maximum free passage diameter, mm**	**Capacity, liters per minute**	**Spray angle, °**	**Material**
Small nozzle B1/4HH-10/ SSC-2036	6.35	3.2	1.6	5.4	67	Brass
Medium nozzle B3/8HH-SS22/SSC-2086	9.52	4.5	2.8	11.9	90	Stainless steel
Big nozzle B1/2HH-40/SSC-2116	12.7	6.2	3.6	21	91	Brass

Maximum free passage diameter in above table is the maximum diameter of foreign matter that can pass through the nozzle without clogging.

The small nozzle used in the experiments is shown in Figure 7.2.

Figure 7.2. Pressure-swirl full cone nozzle B1/4HH-10 used in the experiments (Industrial hydraulic spray products. Catalog 75A-M HYD, 2015, p. B5).

7.2 Initial data for experiment

The measurements were conducted in a square area of 55x50mm on the centerline of a spray cone at pressure of 1 bar in a supply pipe. The water temperature in a supply pipe had a constant value of 10.2 °C. The focal ratio of used lens was f/2.8. Images of sprays were taken at recording frequency of 5 Hz that was estimated (after test experiment) to be enough to get different droplets on successive images.

Working distances are presented in Table 7.2.

Table 7.2. Working distances.

Horizontal distance between camera and the measurement area	Horizontal distance between diffuser and the measurement area	Vertical distance between nozzle orifice and the center of the measurement area
0.6 m	0.31 m	11 cm

7.3 Shadowgraphy system

The visualization and sizing of the droplets in a spray were conducted with the use of LaVision's Shadowgraphy system in connection with DaVis 8.2 data processing software. This setup refers to optical imaging analyzers and uses shadowgraphy technique (backlighting). This technique is based on high resolution imaging with pulsed backlight illumination, as illustrated in Figure 7.3. (Product manual for DaVis 8.2, 2013, p. 9)

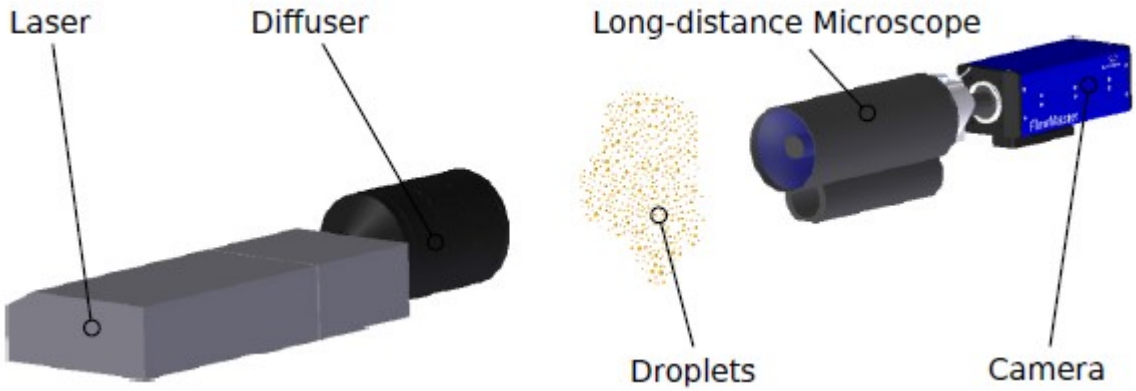

Figure 7.3. Shadowgraphy system. (Ibid.)

A laser generated narrow beam of light with diffuser scattering the light and producing larger area of backlight illuminating the droplets. The light shone towards the camera

creating a white image, the droplets passed between the light and the camera blocking the light path and creating the sharp shadows on the image. The measurements were conducted in a limited volume of a spray defined by the focal plane and the depth of field of the imaging system. A double-pulse laser in combination with a double-frame camera also allowed to determine droplet velocities. Thus, this technique provided information on droplet sizes, shapes and velocities. (Ibid.)

7.4 Basics of the sizing algorithm

Droplet sizes are determined applying thresholding two step segmentation algorithm to the images. The segmentation is performed on the inverted images, where droplets have high intensities whereas the background has low intensities. Inverted images are obtained by subtracting the shadow images from the reference image, as illustrated in Figure 7.4. The reference image represents the illuminated background without droplets. (Product manual for DaVis 8.2, 2013, pp. 9, 10)

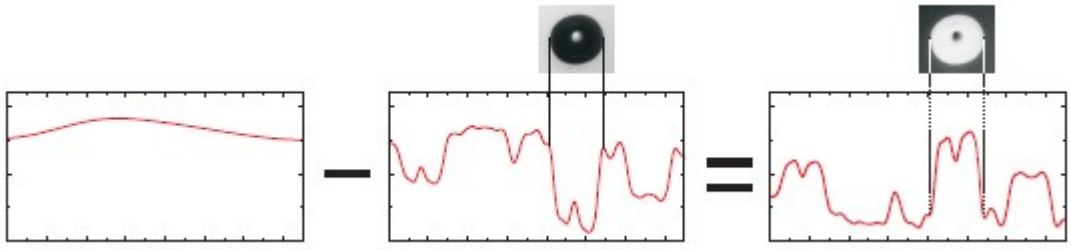

Figure 7.4. Inverting the shadow image. (Product manual for DaVis 8.2, 2013, p. 10)

During the first segmentation the particle recognition is done by applying the user-defined global threshold as a percentage of the difference between maximum and minimum intensity of the inverted images. Intensity profile of an inverted droplet image with the corresponding threshold values for the first segmentation are presented in Figure 7.5. The algorithm analyzes the inverted images, finds coherent pixels with intensities above the global threshold and places them into bounding boxes, which are taken into account for the second segmentation. (Product manual for DaVis 8.2, 2013, pp. 10, 11)

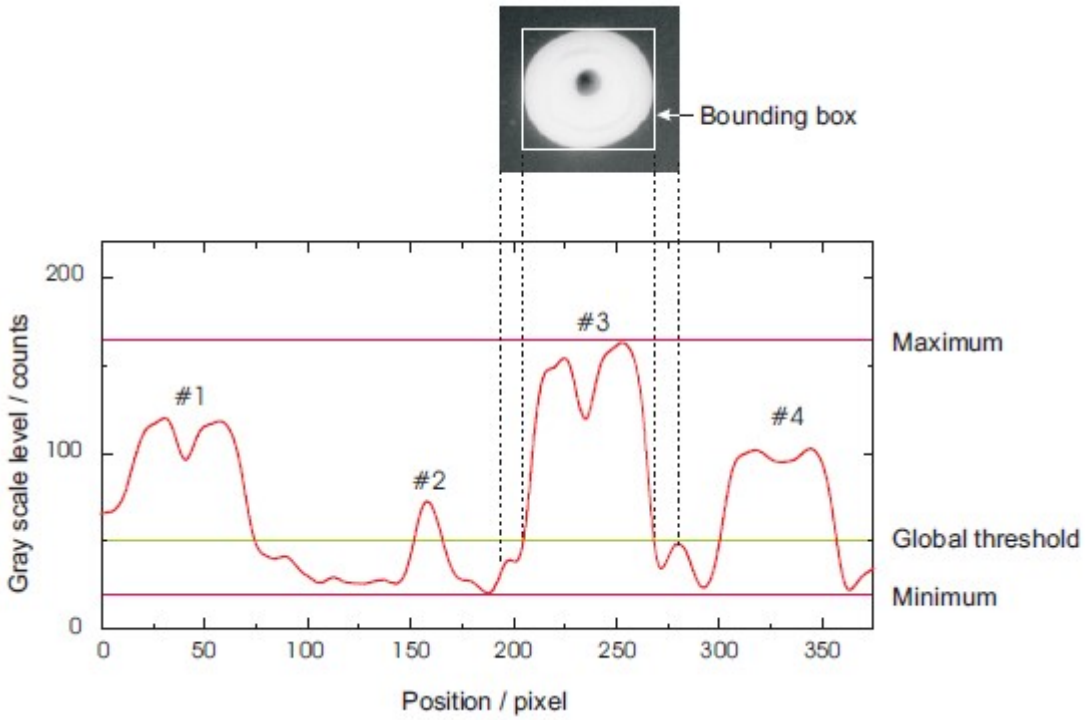

Figure 7.5. Thresholds for the first segmentation (Ibid.)

If no droplets are inside the image, algorithm considers noise as the droplets. In order to avoid it, a second absolute threshold called the minimum shadowing is applied to the images. The value for the minimum shadowing is set by the user based on the intensities of the source images. An image without droplets is shown in Figure 7.6. Here the value of minimum shadowing is higher that the global threshold preventing the algorithm from further processing of this image. (Product manual for DaVis 8.2, 2013, p. 11)

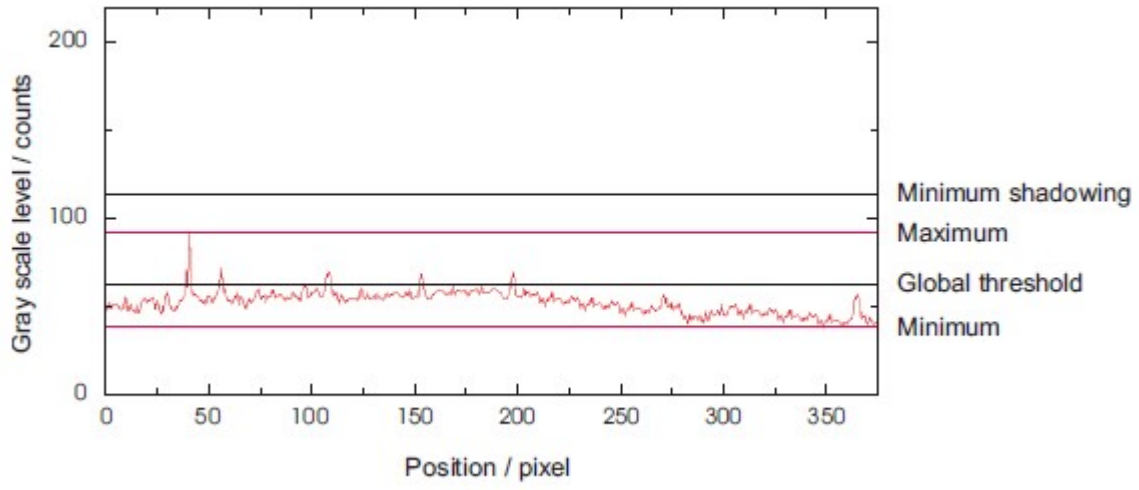

Figure 7.6. Minimum shadowing for the first segmentation. (Ibid.)

The second segmentation is done with each droplet arranged in the bounding box during the first segmentation separately. The user has to define a high and a low level as a percentage of the minimum and maximum intensities in the bounding box, as shown in Figure 7.7 exemplarily for particle №3 from Figure 7.5. (Product manual for DaVis 8.2, p. 12)

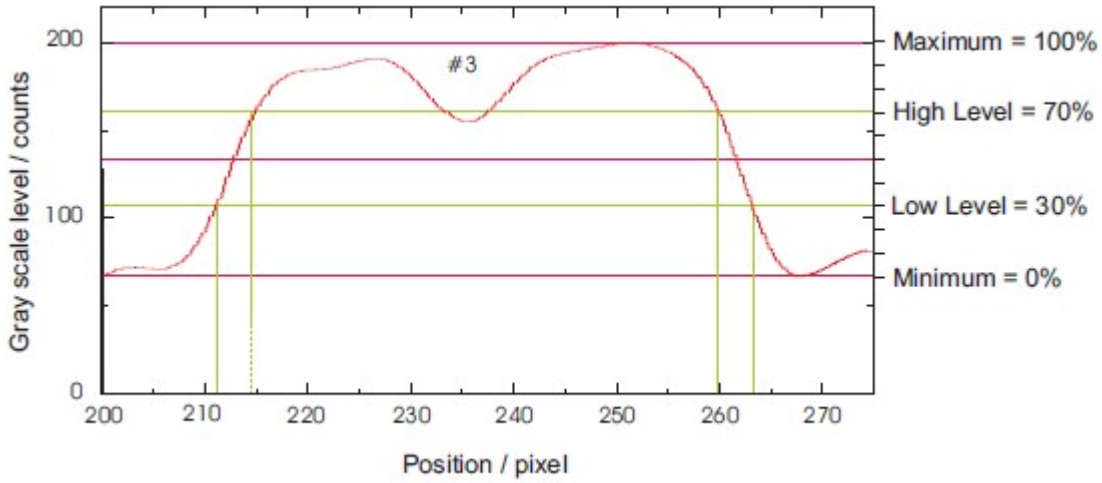

Figure 7.7. Thresholds for the second segmentation. (Ibid.)

The algorithm counts the number of pixels which have intensities above high (nPixHigh) and above low (nPixLow) levels. Then algorithm successively calculates the following values:

1. Droplet areas from the values for nPixHigh and nPixLow;
2. Longest and shortest axis and corresponding circle diameters (assuming a droplet to be a circle of that area);
3. Center of mass, droplet diameter and eccentricity as average of both levels (Ibid.)

8 RESULTS

8.1 Treatment of experimental droplet size data

As an output data DaVis creates text file containing information about droplet diameters, velocities, centricities, etc. Those files were extracted from DaVis project working folder and used in Excel for making statistics and plotting all necessary distributions and graphs. Since there is no reliable information on necessary and sufficient sample size, at first it is necessary to define the minimum number of samples adequately describing droplet population from statistical point of view. It can also help to save time and disk memory in future experiments with the same nozzles. For that purpose, 1000 images were taken for each nozzle, convergence charts for arithmetic mean diameter D_{10} were plotted in Mathcad, which also made it possible to check if droplets were recognized and sized correctly by DaVis. *Y*-axis represents values for D_{10} calculated using successively increasing number of droplets plotted on *X*-axis. These charts are illustrated in Figures 8.1, 8.2, 8.3.

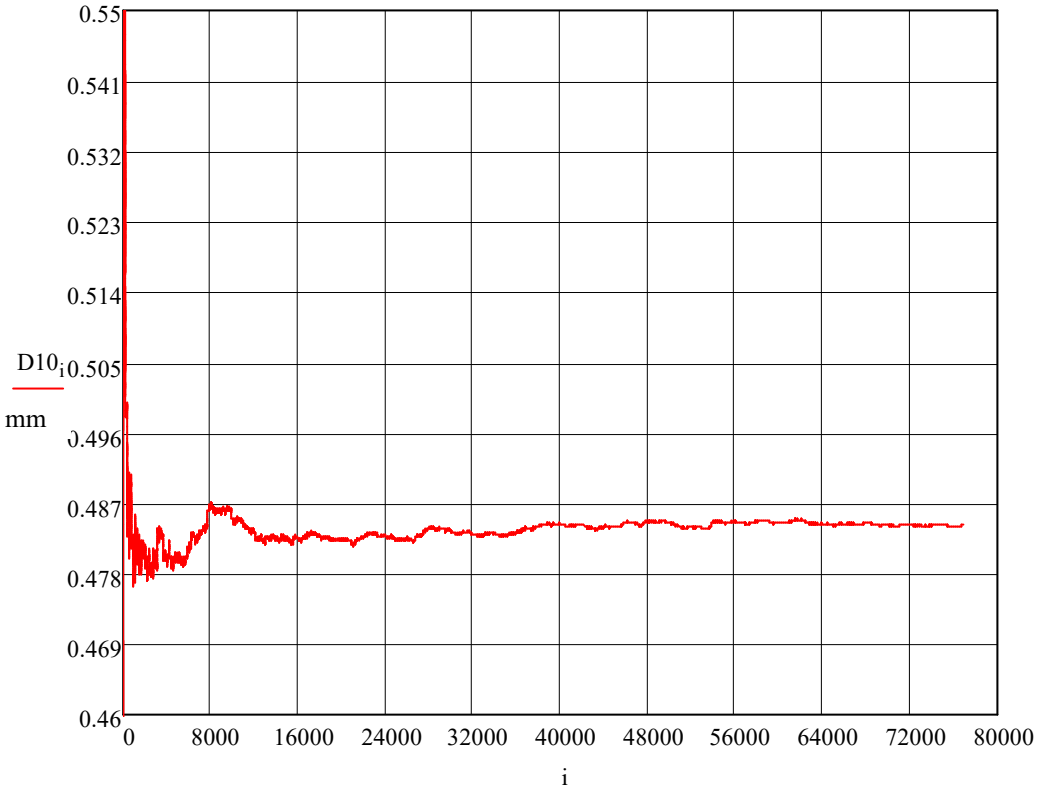

Figure 8.1. Convergence chart for D_{10} of the small nozzle.

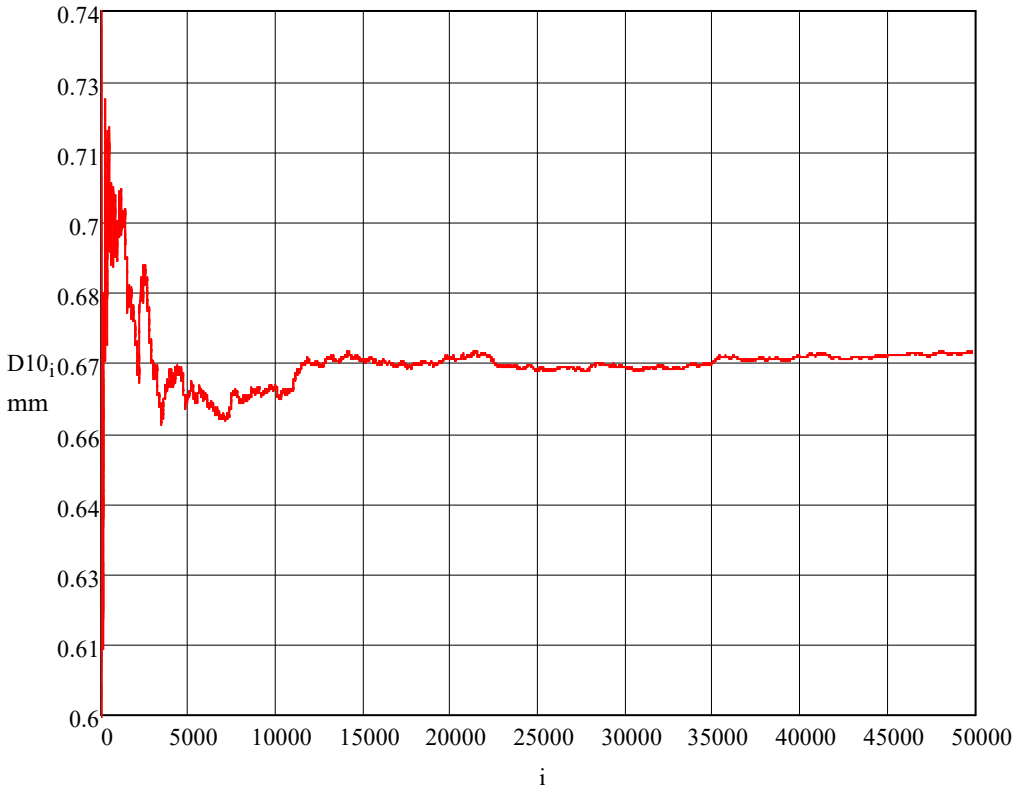

Figure 8.2. Convergence chart for D_{10} of the medium nozzle.

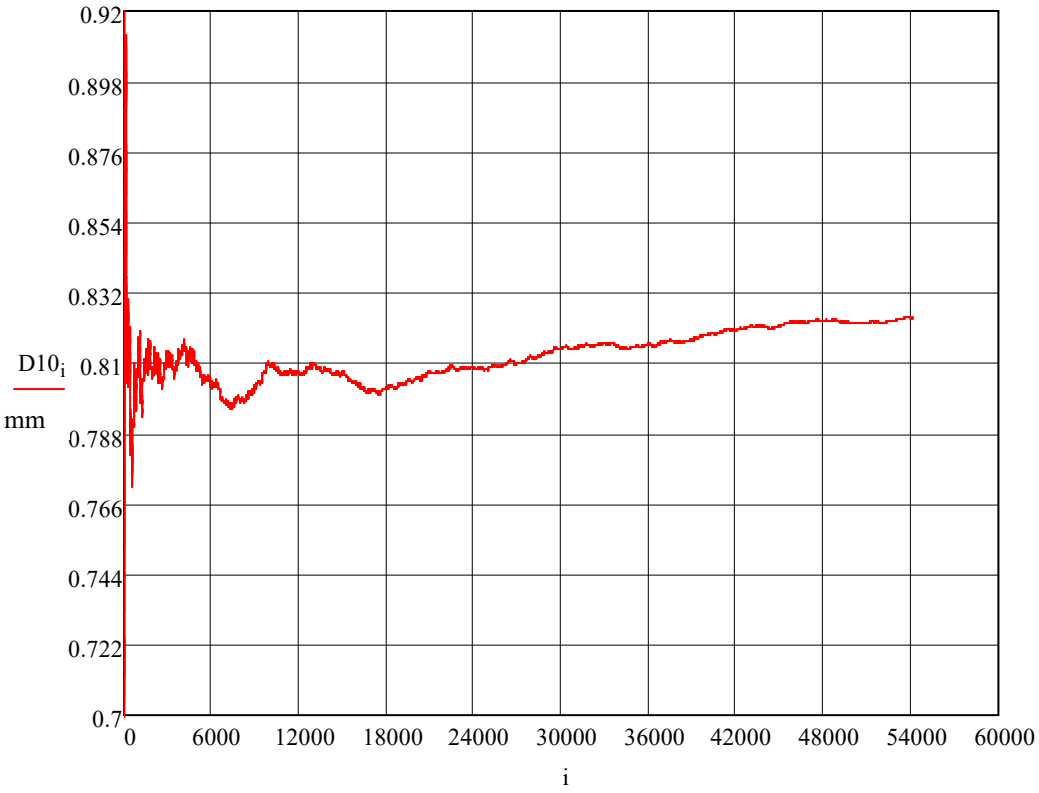

Figure 8.3. Convergence chart for D_{10} of the big nozzle.

As can be seen D_{10} for small and medium nozzles converges well and stays almost the same after number of droplets under consideration reaches 40000. This implies that 40000 of droplets provide adequate statistical information about droplet population. Whereas D_{10} for big nozzle oscillates up to 18000 and diverges afterwards. Obviously, there must be some inaccuracies or faults in droplet sizing done by DaVis which could be checked and fixed manually. For that purpose, droplet data for big nozzle was sorted in the order of decreasing diameter and the biggest droplet from the list (with diameter of *8.34 mm*) was found on processed image №755. This image is presented in Figure 8.4.

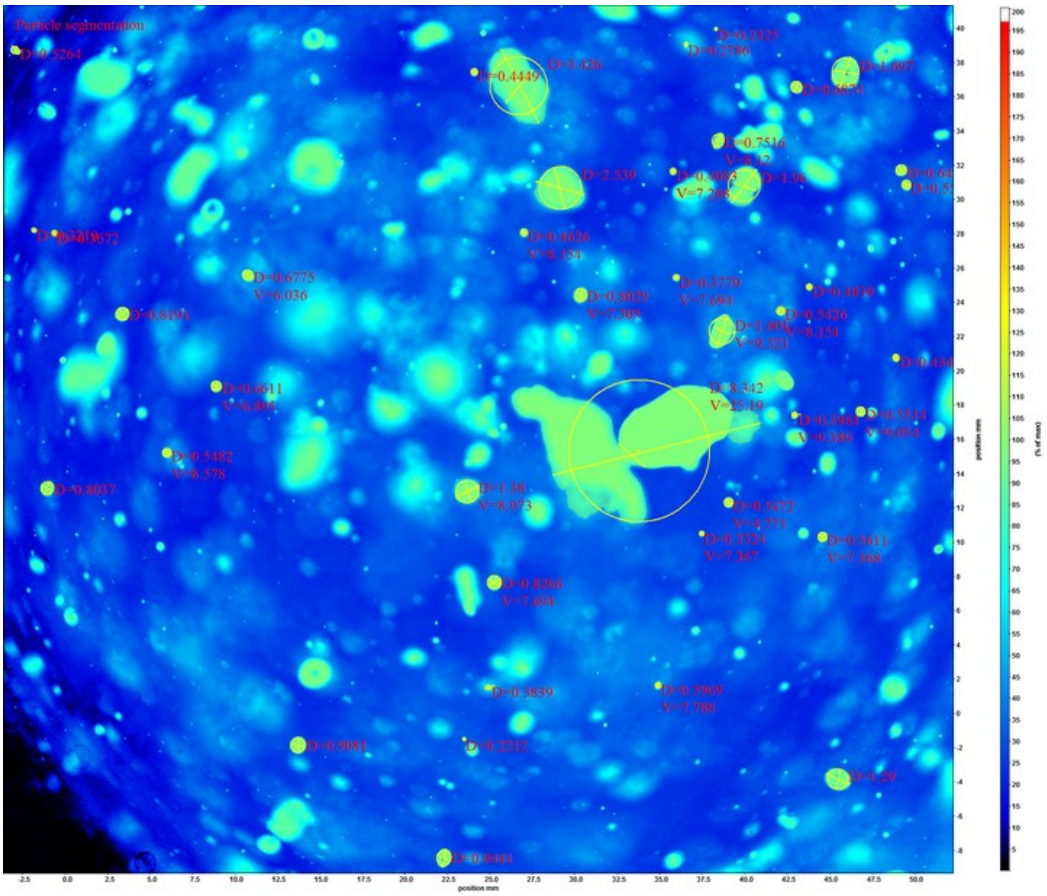

Figure 8.4. Processed image №755 of the big nozzle spray flow.

As it is seen this “droplet” is ligament in reality and must have not been taken into account and sized at all. Some other biggest “droplets” from the sorted droplet data were also found and checked on the images and also turned out to be ligaments. Since manual check through all the droplets takes a lot of time considering 1000 images it was decided to introduce some “rule of thumb” that keeps only droplets and no ligaments. One visible

common characteristic of those ligaments is small value of centricity. In order to eliminate ligaments from droplet data it was decided to exclude all the droplets with centricity less than *0.75* but still keep droplets complying with this rule (i.e. with centricity less than *0.75*) with diameter less than *3 mm* (value for the border diameter was chosen manually by looking at the set of processed images). These operations were easily done by sorting function of Excel. Even though D_{10} converges for small and medium nozzle, it was decided to do the same filtering for them as well but with different values of border diameter (*2 mm* for small and *2.5 mm* for medium nozzle). Converging charts after filtering of the droplet data are illustrated in Figures 8.5, 8.6, 8.7 (droplets were sorted back to the original order).

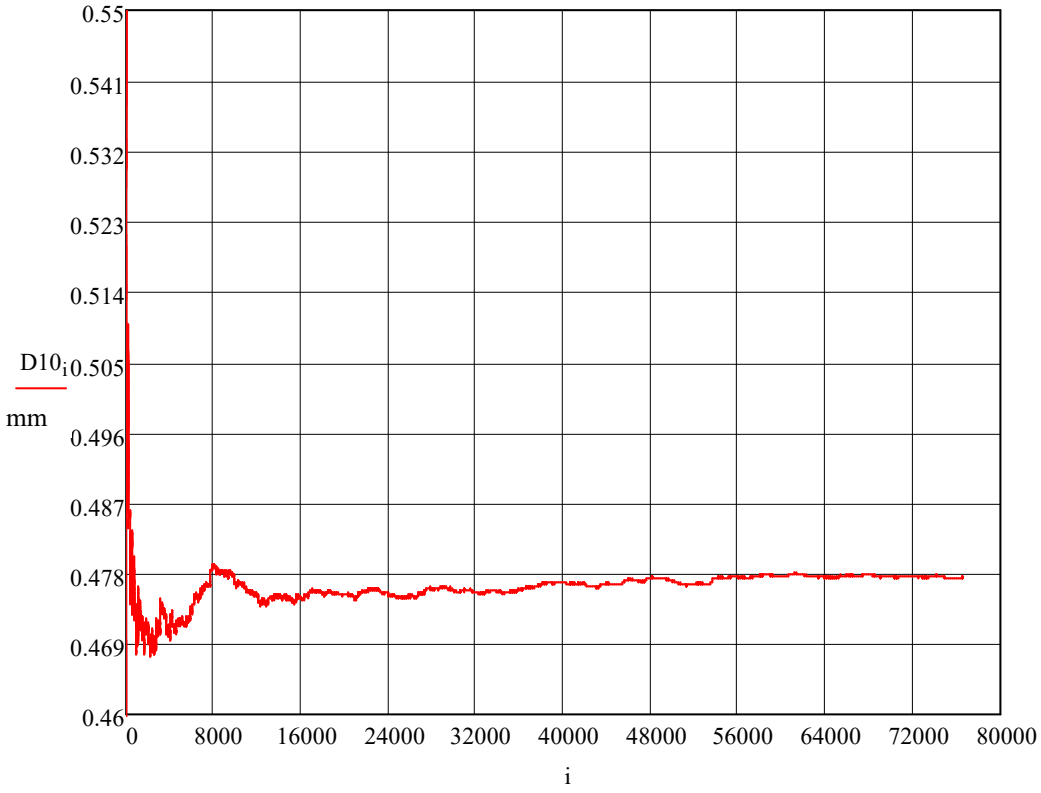

Figure 8.5. Convergence chart for D_{10} of the small nozzle after filtering of the data.

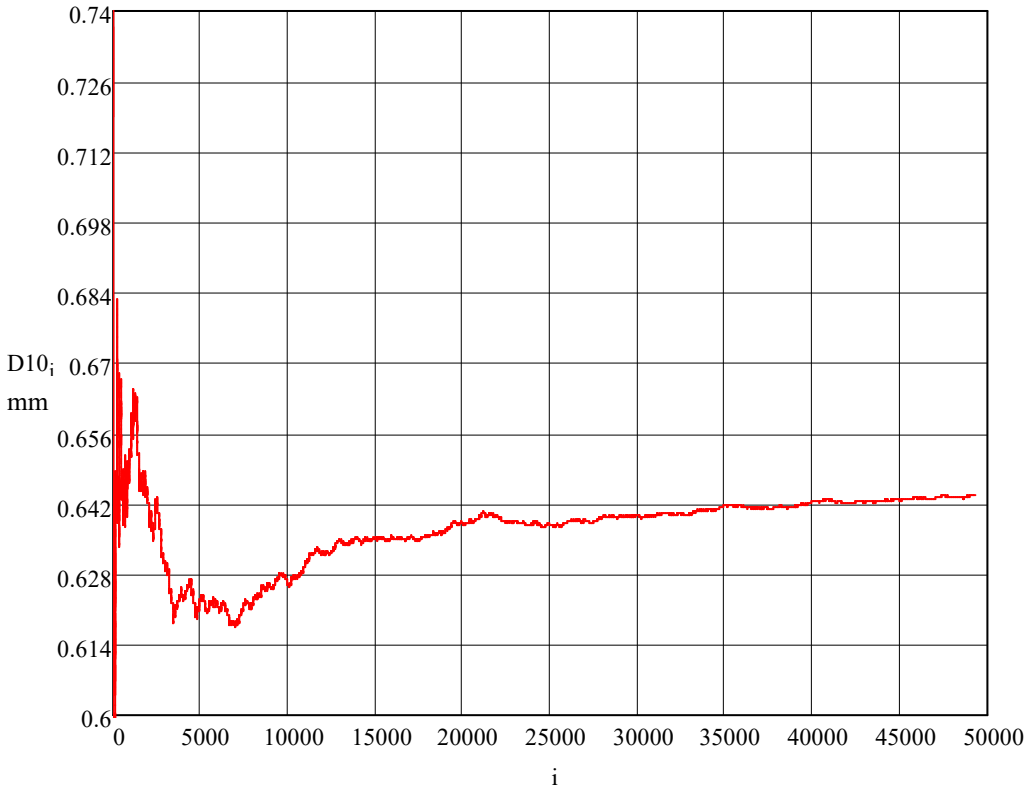

Figure 8.6. Convergence chart for D_{10} of the medium nozzle after filtering of the data.

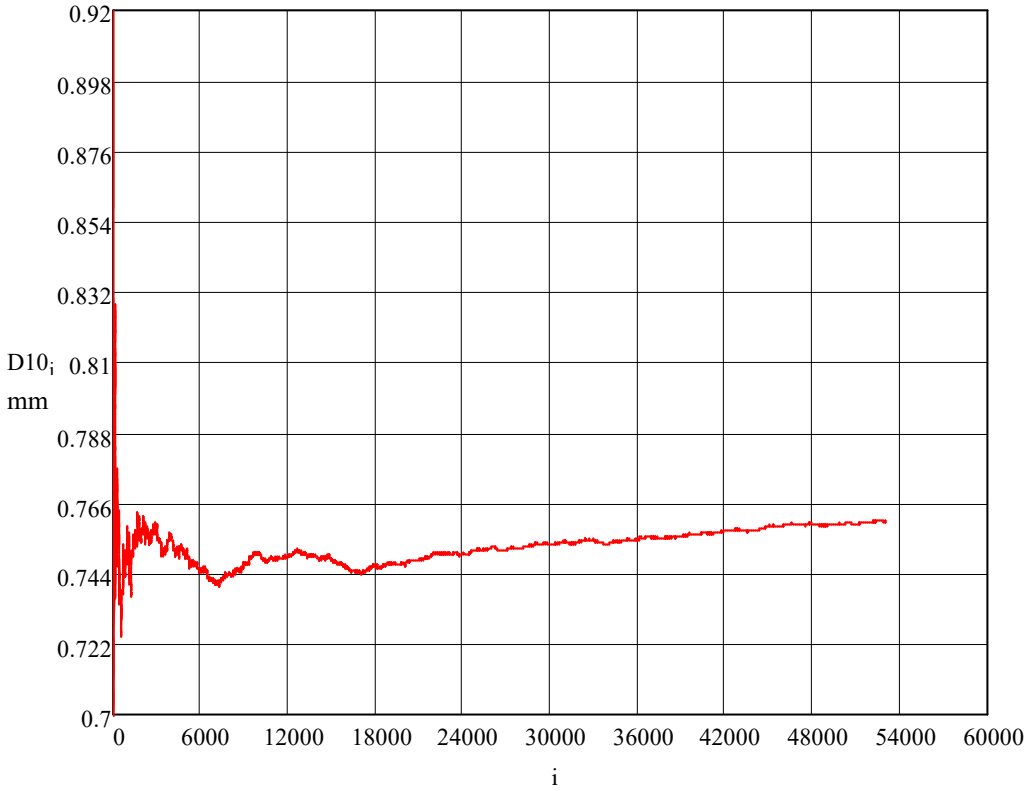

Figure 8.7. Convergence chart for D_{10} of the big nozzle after filtering of the data.

It's seen that now frequency of oscillations decreased on all charts and mean values for them also decreased since many large ligaments were filter out. As a main result the chart for big nozzle converges better in the region of 40000 droplets.

Thus, in our case 40000 of droplets are considered to be enough to get good statistics, since the amplitude of oscillations of D_{10} is negligibly small. The obtained errors are defined as follows:

$$Err = \left| \frac{D_{10\,i-1} - D_{10\,i}}{D_{10\,i}} \right|, \tag{8.1}$$

where D_{10i-1} – arithmetic mean diameter calculated using *i-1* droplets, D_{10i} – arithmetic mean diameter calculated using *i* droplets, are presented in Table 8.1.

Table 8.1. Convergence errors of D_{10}.

	Small nozzle	**Medium nozzle**	**Big nozzle**
Err	$9.563 \cdot 10^{-6}$	$4.428 \cdot 10^{-5}$	$1.306 \cdot 10^{-5}$

Hence, the future discussion will be referred to 40000 droplets. In order to show adequacy of obtained droplet data, convergence charts for D_{32} were also plotted and presented in Figures 8.8, 8.9, 8.10.

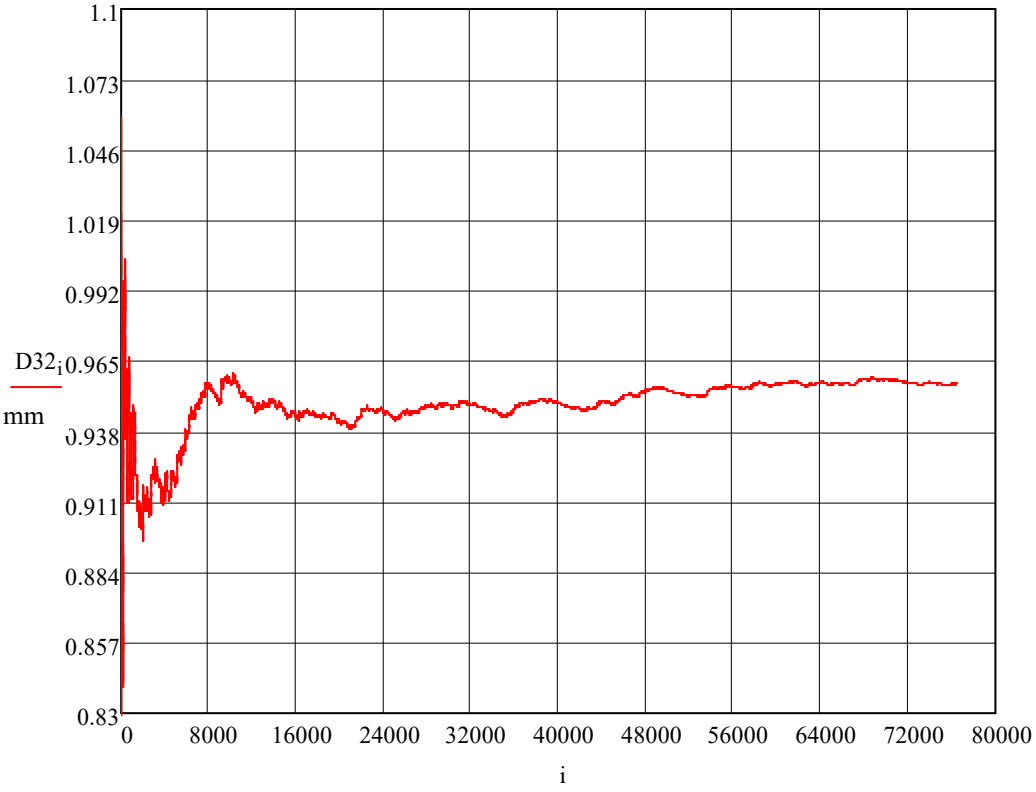

Figure 8.8. Convergence chart for D_{32} of the small nozzle after filtering of the data.

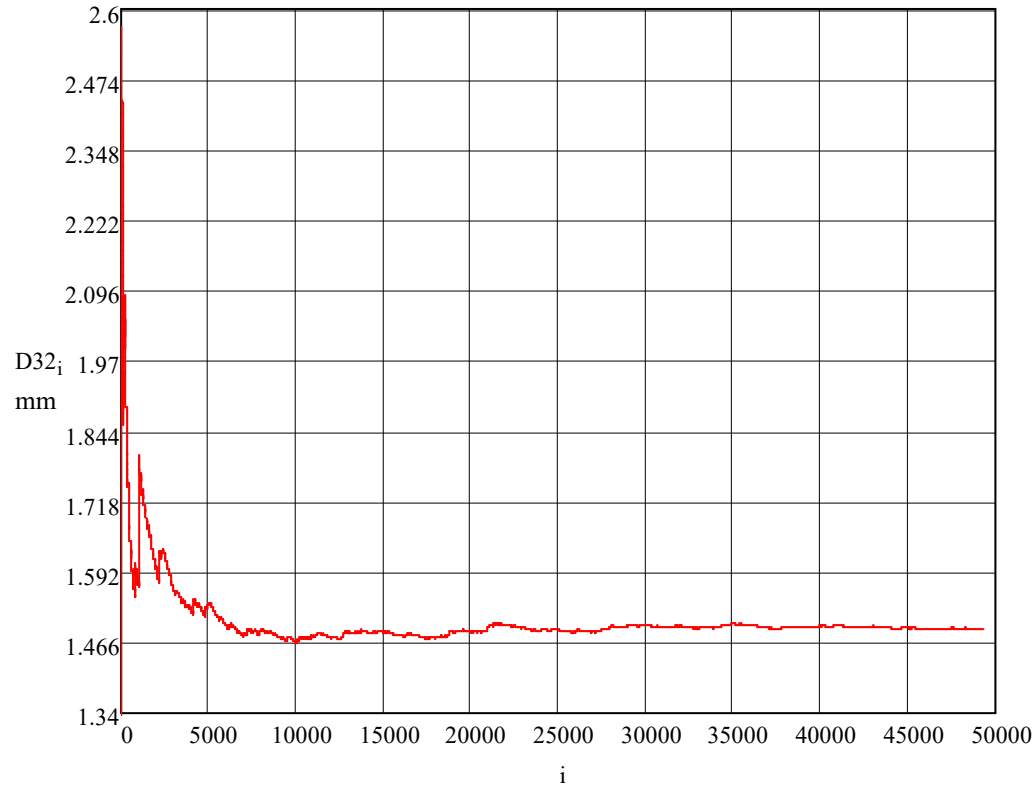

Figure 8.9. Convergence chart for D_{32} of the medium nozzle after filtering of the data.

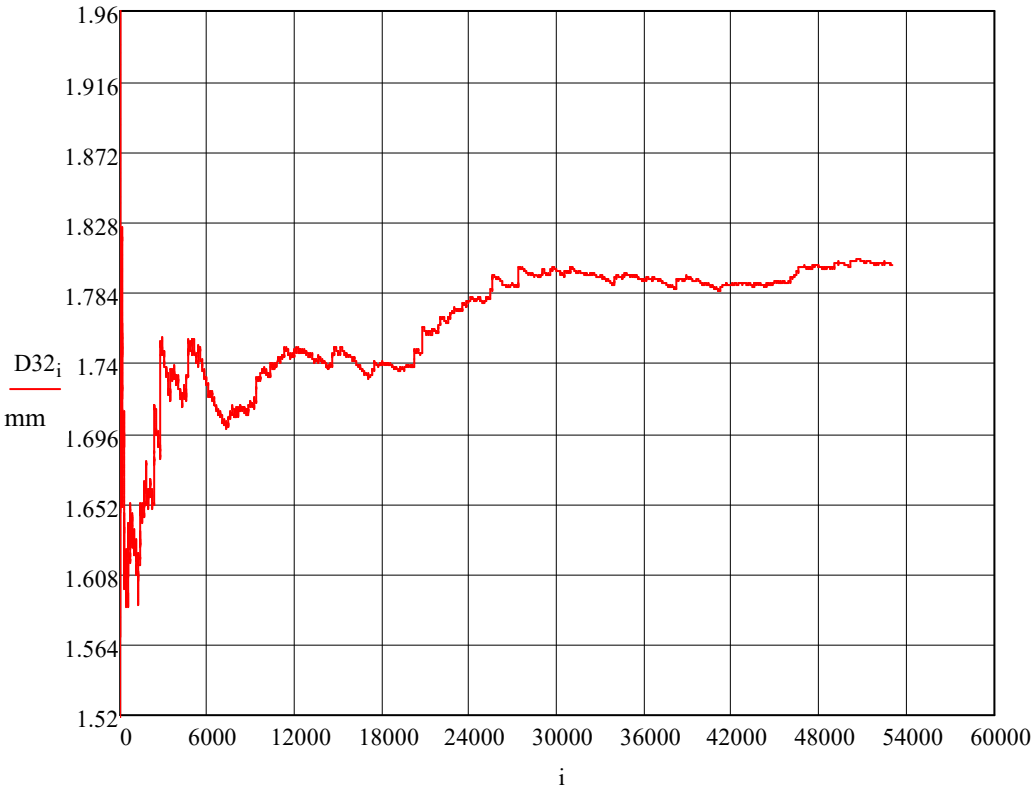

Figure 8.10. Convergence chart for D_{32} of the big nozzle after filtering of the data.

Corresponding errors defined similarly as in Eq. (8.1) are presented in Table 8.2.

Table 8.2. Convergence errors of D_{32}.

	Small nozzle	**Medium nozzle**	**Big nozzle**
Err	$4.686 \cdot 10^{-6}$	$2.339 \cdot 10^{-5}$	$2.832 \cdot 10^{-6}$

8.2 Processing of experimental droplet size data

Experimental droplet size frequency distributions are presented in the form of histograms as discussed in Chapter 2.2. Width of ΔD interval in Eqs. (3.1) and (3.4) is chosen automatically by Excel and equal to $0.016\ mm$.

Rosin-Rammler and Nukiyama-Tanasawa theoretical droplet size frequency distributions described in Chapters 3.3.1, 3.3.2 were applied in order to fit experimental data. Those were used in the forms derived in (González-Tello, et al., 2008, p. 279) which is discussed below.

Rosin-Rammler droplet volume frequency distribution is obtained by differentiation of (3.6):

$$f_V(D) = \frac{n}{m}\left(\frac{D}{m}\right)^{n-1} \exp\left(-\left(\frac{D}{m}\right)^n\right), \tag{8.2}$$

Rosin-Rammler droplet number frequency distribution, $f_N(D)$, can be derived considering normalization conditions:

$$\int_{D_{\min}}^{D_{\max}} f_N(D)dD = 1, \qquad \int_{D_{\min}}^{D_{\max}} f_N(D)dD = 1, \tag{8.3}$$

and correlation between $f_V(D)$ and $f_N(D)$:

$$f_V(D) = \frac{D^3 f_N(D)}{\int_{D_{\min}}^{D_{\max}} D^3 f_N(D)dD}, \tag{8.4}$$

yielding:

$$f_N(D) = \frac{n}{m\Gamma\left(\frac{n-3}{n}\right)}\left(\frac{D}{m}\right)^{n-4} \exp\left(-\left(\frac{D}{m}\right)^n\right), \tag{8.5}$$

Nukiyama-Tanasawa droplet number and droplet volume frequency distributions are obtained by applying Eqs. (8.3) and (8.4) and doing some more mathematical derivations with Eq. (3.7), yielding:

$$f_N(D) = \frac{n}{D_{32}\Gamma\left(\frac{p+1}{n}\right)}\left(\frac{\Gamma\left(\frac{p+4}{n}\right)}{\Gamma\left(\frac{p+3}{n}\right)}\right)^{p+1}\left(\frac{D}{D_{32}}\right)^p \exp\left(-\left(\frac{\Gamma\left(\frac{p+4}{n}\right)}{\Gamma\left(\frac{p+3}{n}\right)}\right)^n\left(\frac{D}{D_{32}}\right)^n\right), \tag{8.6}$$

$$f_V(D) = \frac{n}{D_{32}\Gamma\left(\frac{p+4}{n}\right)}\left(\frac{\Gamma\left(\frac{p+4}{n}\right)}{\Gamma\left(\frac{p+3}{n}\right)}\right)^{p+4}\left(\frac{D}{D_{32}}\right)^{p+3} \exp\left(-\left(\frac{\Gamma\left(\frac{p+4}{n}\right)}{\Gamma\left(\frac{p+3}{n}\right)}\right)^n\left(\frac{D}{D_{32}}\right)^n\right). \tag{8.7}$$

where n, p – constant parameters, m – droplet diameter such that 63.2% of the total liquid volume is in the droplets of smaller diameter, Γ – gamma function, D_{32} – Sauter mean diameter.

Droplet mass fraction frequency distributions are of interest for Computational Fluid Dynamics code ANSYS Fluent because they are used (rather than droplet number frequency distributions) as a reference data to set spray injections of a modelled nozzle (ANSYS Fluent User's Guide, 2013, p. 1171). It should be noted, that considering constant

value of water density, the droplet mass fraction distribution coincides with the droplet volume frequency distribution.

Values of m and D_{32} in Eqs. (8.2), (8.5), (8.6), (8.7) were calculated after processing of experimental droplet data with Excel and presented in Table 8.3.

Table 8.3. Values of m and D_{32}.

	Small nozzle	**Medium nozzle**	**Big nozzle**
m, mm	*1.45*	*2.21*	*2.55*
D_{32}, mm	*0.95*	*1.49*	*1.79*

Constant n in Eqs. (8.2), (8.5) and two constants n and p in Eqs. (8.6), (8.7) were used to find the best-fit of experimental data. Absolute Mean Average Deviation (*AMAD*) and Residual Sum of Squares (*RSS*) were applied as optimality criteria (González-Tello, et al., 2008, pp. 280, 281):

$$AMAD = \frac{1}{N}\sum_{i=1}^{N}\left|\frac{f(D)_{\exp} - f(D)_{calc}}{f(D)_{\exp}}\right|, \tag{8.8}$$

$$RSS = \frac{1}{N}\sum_{i=1}^{N}\left(f(D)_{calc} - f(D)_{\exp}\right)^2 \quad , \tag{8.9}$$

where $f(D)_{\exp}$/$f(D)_{\text{calc}}$ – experimental/calculated value of frequency distribution function, N – total number of droplets.

Rosin-Rammler droplet number frequency distribution has the following multiplier in Eq. (8.5)

$$f(n) = \frac{1}{\Gamma\left(\frac{n-3}{n}\right)}, \tag{8.10}$$

whose graph is presented in Figure 8.11. This function was manually studied for its domain of definition and it was found that it is not defined or goes to infinity at $n \in (0\text{-}0.06)$ and $n=(0.1, 0.12, 0.15, 0.2, 0.25, 0.3, 0.5, 0.6, 1, 1.5, 3)$.

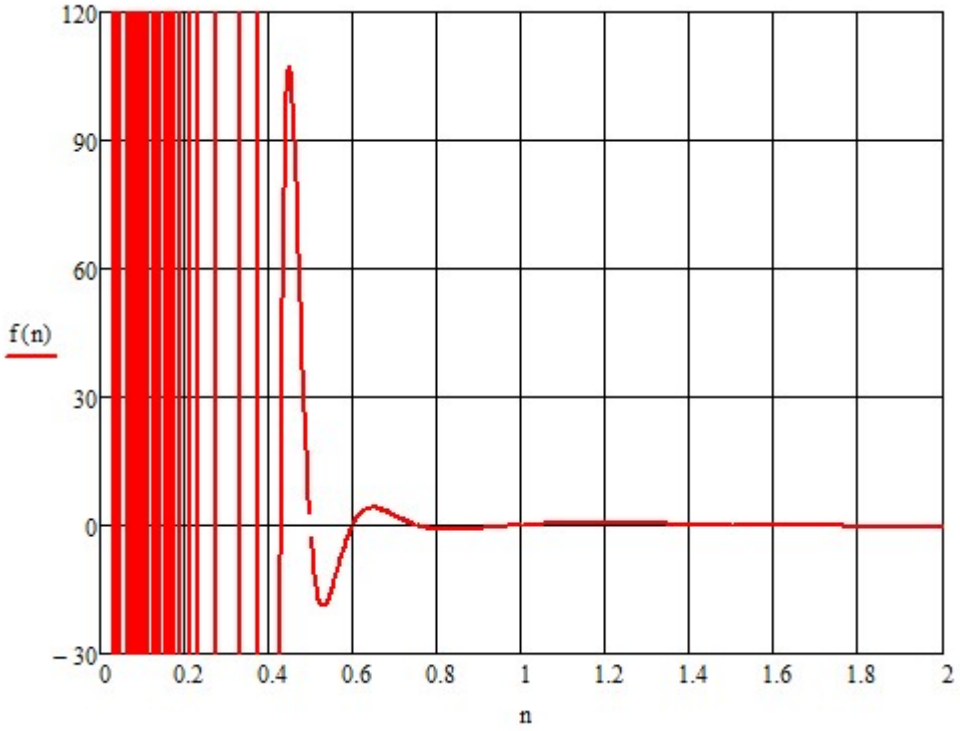

Figure 8.11. Graphical representation of gamma function multiplier *f(n)* in Eq. (8.5).

Specially written Mathcad program calculated the values of *AMAD* and *RSS* at different values of *n* ranging from *0.11* to *10* with step of *0.1* (chosen values enable staying within the domain of definition) in Eqs. (8.2), (8.5); and at different combinations of *n* and *p* both ranging from *0.1* to *10* with step of *0.1* in Eqs. (8.6), (8.7) with following finding of minimum values of *AMAD* and *RSS* and corresponding values of *n* and *p*.

Since there might be a need to use both droplet number and volume frequency distribution at the same time with the only optimal values of *n* and *p*, Mathcad program also calculated combined optimality criteria defined as quadratic mean of two:

$$AMAD_{COMB} = \sqrt{\frac{1}{2}\left(AMAD_N{}^2 + AMAD_V{}^2\right)}, \tag{8.11}$$

$$RSS_{COMB} = \sqrt{\frac{1}{2}\left(RSS_N{}^2 + RSS_V{}^2\right)}. \tag{8.12}$$

The same program was used to find minimum values of errors and corresponding values of *n* and *p* for combined case.

8.3 Results of experiment

Optimal values of *AMAD* and *RSS* and corresponding values of *n* in Rosin-Rammler and *n* and *p* in Nukiyama-Tanasawa droplet size frequency distributions are presented in Tables 8.4 - 8.9.

Table 8.4. Optimal values of *AMAD* and *RSS* and spread parameter *n* in Rosin-Rammler droplet number and volume frequency distributions of small nozzle.

	$AMAD_N$	$AMAD_V$	$AMAD_{COMB}$	RSS_N	RSS_V	RSS_{COMB}
Error	***0.444***	*0.395*	***0.463***	*0.34*	***0.012***	*0.243*
n	***3.21***	*2.41*	***3.21***	*3.61*	***2.21***	*3.61*

Table 8.5. Optimal values of *AMAD* and *RSS*, *n* and *p* in Nukiyama-Tanasawa droplet number and volume frequency distributions of small nozzle.

	$AMAD_N$	$AMAD_V$	$AMAD_{COMB}$	RSS_N	RSS_V	RSS_{COMB}
Error	*0.349*	*0.368*	*0.359*	***0.071***	***0.015***	***0.052***
n	*1.2*	*1.2*	*1.2*	***0.2***	***0.8***	***0.2***
p	*0.2*	*0.1*	*0.1*	***10***	***0.1***	***10***

Table 8.6. Optimal values of *AMAD* and *RSS* and spread parameter *n* in Rosin-Rammler droplet number and volume frequency distributions of medium nozzle.

	$AMAD_N$	$AMAD_V$	$AMAD_{COMB}$	RSS_N	RSS_V	RSS_{COMB}
Error	***0.48***	***0.31***	***0.492***	*0.102*	$3.363 \cdot 10^{-3}$	*0.073*
n	***3.21***	***2.31***	***3.21***	*3.51*	*2.21*	*3.51*

Table 8.7. Optimal values of *AMAD* and *RSS*, *n* and *p* in Nukiyama-Tanasawa droplet number and volume frequency distributions of medium nozzle.

	$AMAD_N$	$AMAD_V$	$AMAD_{COMB}$	RSS_N	RSS_V	RSS_{COMB}
Error	*0.272*	*0.271*	*0.274*	$\mathbf{9.777 \cdot 10^{-3}}$	$\mathbf{3.817 \cdot 10^{-3}}$	$\mathbf{8.106 \cdot 10^{-3}}$
n	*0.9*	*1*	*0.9*	***0.2***	***0.9***	***0.2***
p	*0.5*	*0.1*	*0.4*	***7.7***	***0.1***	***7.8***

Table 8.8. Optimal values of *AMAD* and *RSS* and spread parameter *n* in Rosin-Rammler droplet number and volume frequency distribution of big nozzle.

	$AMAD_N$	$AMAD_V$	$AMAD_{COMB}$	RSS_N	RSS_V	RSS_{COMB}
Error	***0.523***	***0.401***	***0.515***	*0.06*	$\mathbf{3.584 \cdot 10^{-3}}$	*0.043*
n	***3.21***	***2.51***	***3.21***	*3.51*	***2.51***	*3.51*

Table 8.9. Optimal values of *AMAD* and *RSS*, *n* and *p* in Nukiyama-Tanasawa droplet number and volume frequency distributions of big nozzle.

	$AMAD_N$	$AMAD_V$	$AMAD_{COMB}$	RSS_N	RSS_V	RSS_{COMB}
Error	*0.337*	***0.347***	***0.487***	$\mathbf{3.832 \cdot 10^{-3}}$	$\mathbf{4.247 \cdot 10^{-3}}$	$8.659 \cdot 10^{-3}$
n	*1.1*	***1.2***	***1.1***	***0.2***	***1.2***	*0.2*
p	*0.1*	***0.1***	***0.1***	***7.1***	***0.1***	*7.5*

Tables contain the values optimal for individual distribution (featuring subscript *N/V* for droplet number/volume frequency distribution) and also values simultaneously optimal for both distributions (featuring subscript *COMB*).

Since there are two set of values (depending on optimality criterion – *AMAD* or *RSS*) obtained for each case (*N, V or COMB*), it is necessary to find the better one out of two. For that purpose, *AMAD* value was calculated at values of *n* and *p* optimal for *RSS* and vice versa. Then obtained values of *AMAD*s and *RSS*s (optimal itself and calculated with optimal values of *n* and *p* for the other optimality criterion) were compared and the one which gave smaller relative error was chosen. Final best-fit values of *AMAD* and *RSS*, *n* and *p* are marked with bold in Tables 7.8 - 8.9.

Different best-fit values from Tables 8.8 – 8.9 marked with bold should be used depending on application. In case either droplet number or volume frequency distribution is of interest, individual best-fit values should be used - *N* or *V*; in case they're both of interest at the same time, *COMB* best-fit values should be used. Distributions presented below are plotted with individual best-fit values - *N* and *V*, because they give more accurate fit of either individual case than *COMB* best-fit values.

Experimental droplet number frequency distributions along with best-fit (*N*) Rosin-Rammler and Nukiyama-Tanasawa droplet number distributions are presented in Figures 8.11, 8.12, 8.13.

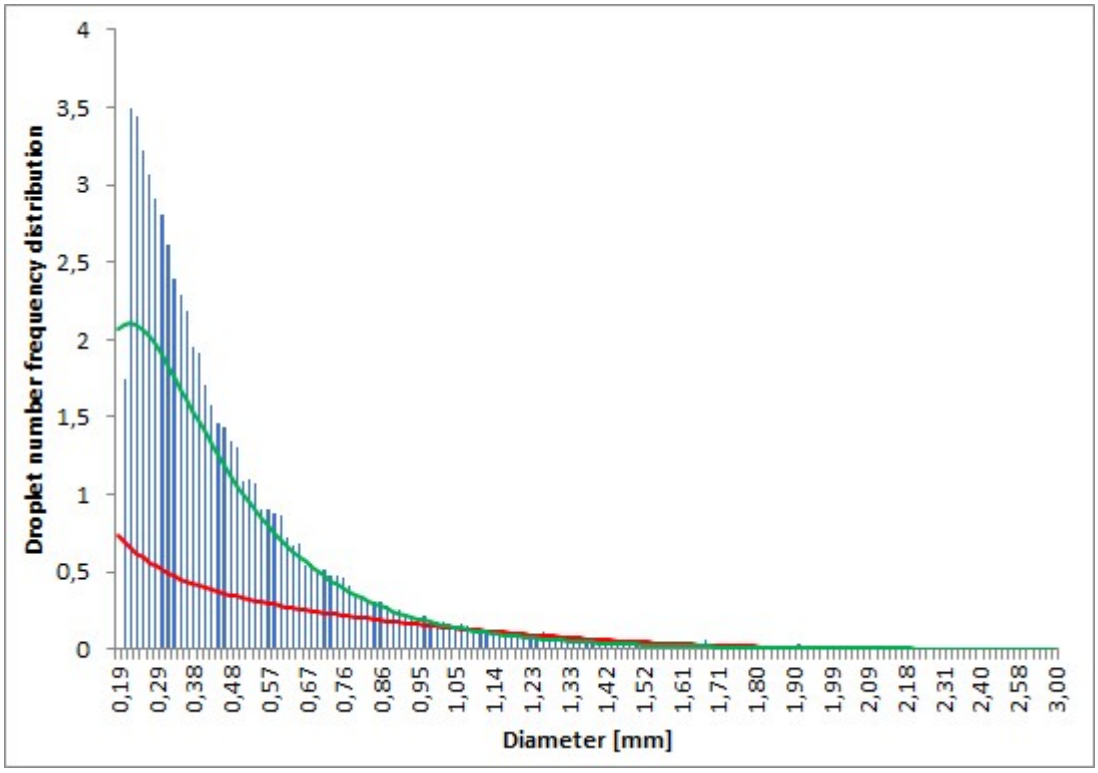

Figure 8.11. Experimental, Rosin-Rammler (red) and Nukiyama-Tanasawa (green) droplet number frequency distributions for small nozzle.

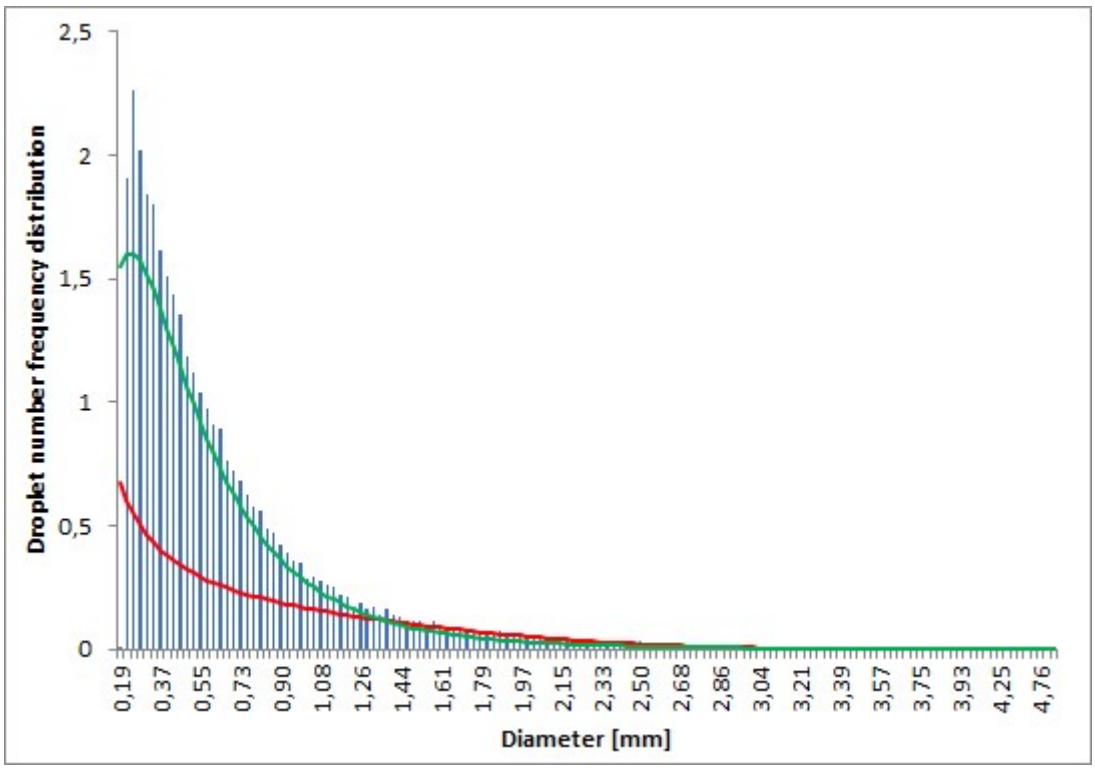

Figure 8.12. Experimental, Rosin-Rammler (red) and Nukiyama-Tanasawa (green) droplet number frequency distributions for medium nozzle.

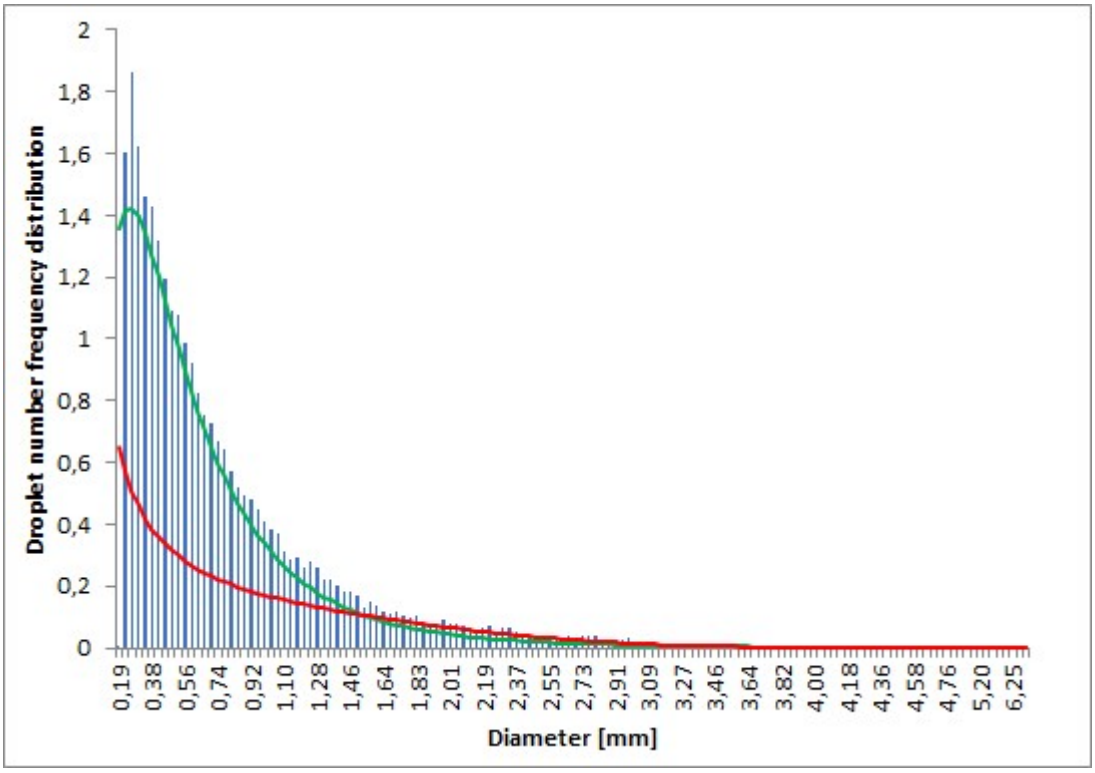

Figure 8.13. Experimental, Rosin-Rammler (red) and Nukiyama-Tanasawa (green) droplet number frequency distributions for big nozzle.

Statistical results on droplet sizes obtained after processing of droplet data with Excel are summarized in Table 8.10.

Table 8.10. Statistical results on droplet sizes.

Parameter	Small nozzle	Medium nozzle	Big nozzle
D_{10}, mm	*0.48*	*0.64*	*0.76*
Standard deviation of D_{10}, mm	*0.30*	*0.48*	*0.59*
D_{20}, mm	*0.56*	*0.80*	*0.96*
D_{30}, mm	*0.67*	*0.99*	*1.18*
D_{32}, mm	*0.95*	*1.49*	*1.79*
$D_{0.1}$, mm	*0.52*	*0.84*	*1.06*
$D_{0.5}$, mm	*1.23*	*1.91*	*2.22*
$D_{0.9}$, mm	*1.94*	*3.27*	*3.60*

The main parameter influencing droplet sizes in our experiments is water flow rate through the nozzle. Small nozzle with the lowest water flow rate generates droplets with the smallest diameters ranging from *0.19 mm* to *3.00 mm* with arithmetic mean diameter D_{10} equal to *0.48 mm*, and as seen from statistical results, 90% of total liquid volume is in

droplets of smaller than *1.94 mm* (parameter $D_{0.9}$). Increase in water flow rate broadens the range of droplet diameters and for medium and big nozzles they vary from *0.19 mm* to *4.76 mm* and from *0.19 mm* to *6.25 mm* correspondingly, resulting in arithmetic mean diameters equal to *0.64 mm* and *0.76 mm* correspondingly. Similar tendency can be seen with surface mean, D_{20}, and volume mean, D_{30}, diameters. (see Table 8.10).

Therefore, increasing the water flow rate at a certain pressure value leads to growth in arithmetic, surface and volume mean diameters. It can be explained by the fact that at a certain pressure value droplets of the nozzle with the higher water flow rate have lower mean velocity. Consequently, both external aerodynamic and internal turbulent disrupting forces act at a lower extent, which leads to larger mean diameters.

Experimental droplet volume frequency distributions along with best-fit (*V*) Rosin-Rammler and Nukiyama-Tanasawa droplet volume frequency distributions are presented in Figures 8.14, 8.15 and 8.16.

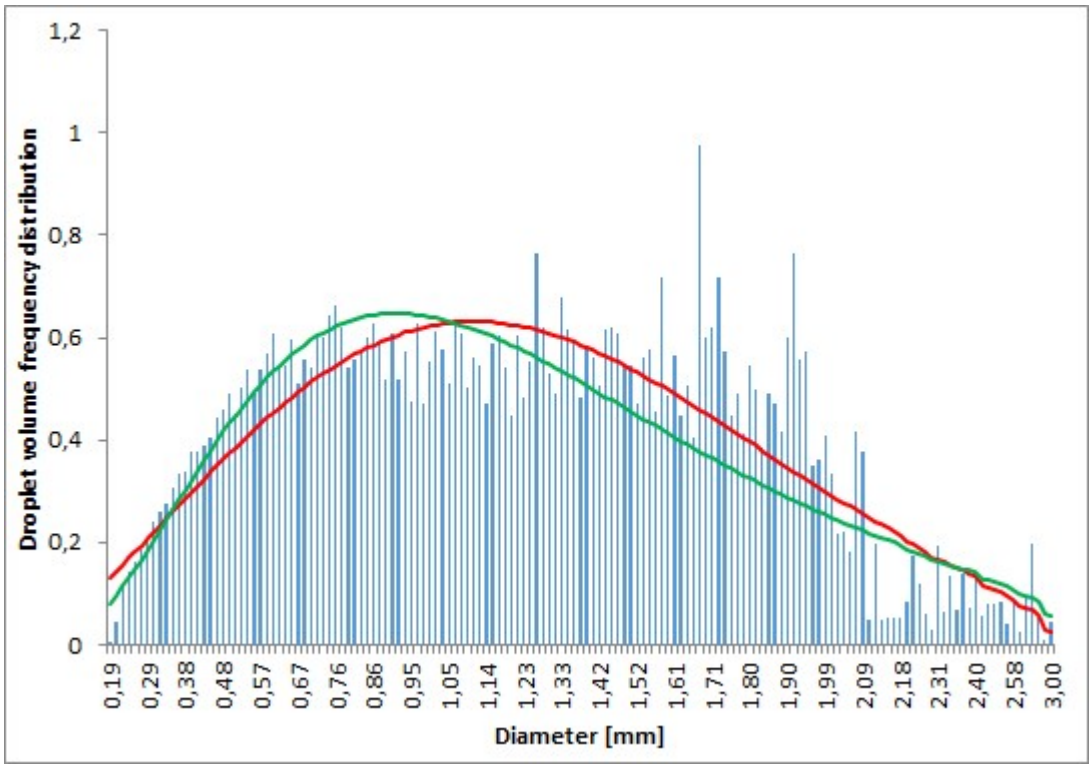

Figure 8.14. Experimental, Rosin-Rammler (red) and Nukiyama-Tanasawa (green) volume frequency distributions for small nozzle.

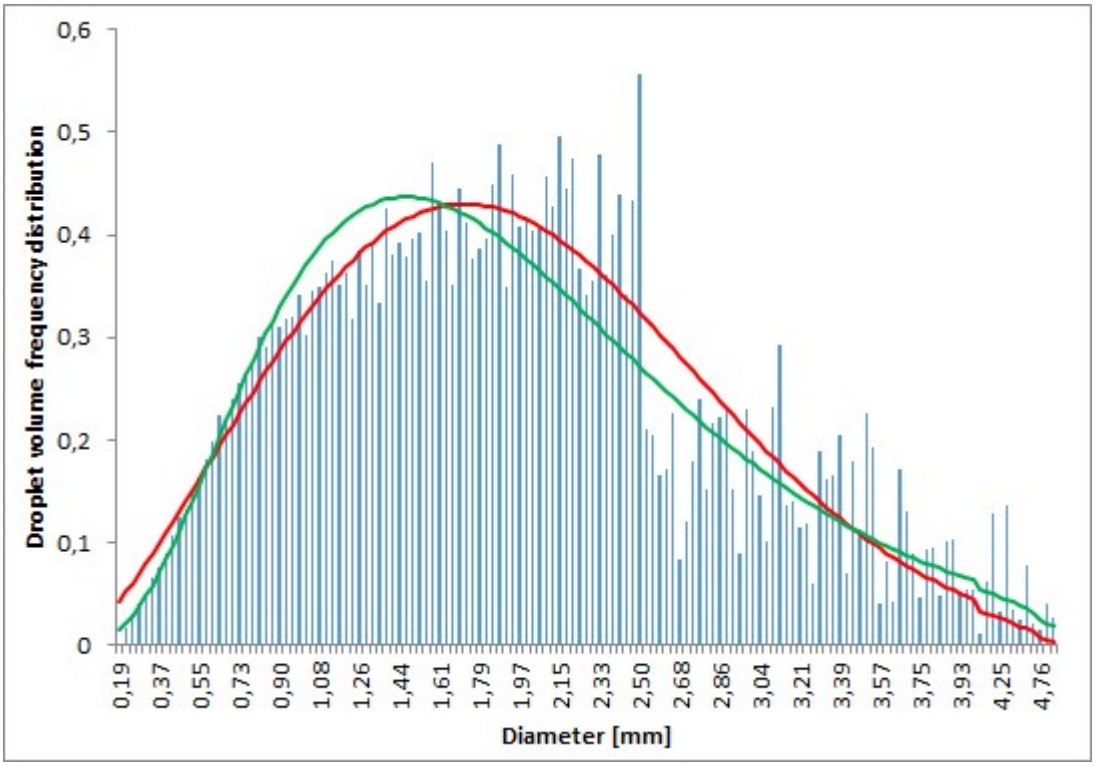

Figure 8.15. Experimental, Rosin-Rammler (red) and Nukiyama-Tanasawa (green) volume frequency distributions for medium nozzle.

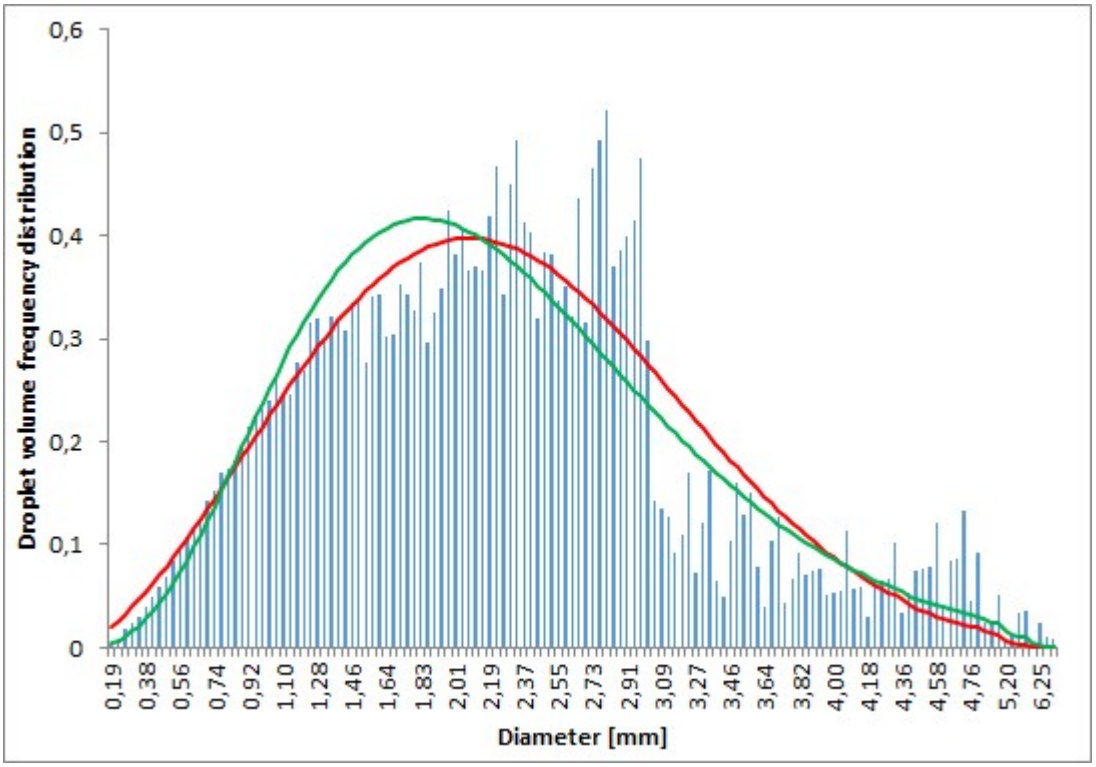

Figure 8.16. Experimental, Rosin-Rammler (red) and Nukiyama-Tanasawa (green) volume frequency distributions for big nozzle.

It is seen that experimental droplet volume frequency distributions are skewed to the right in relation to droplet number frequency distribution because of the weighting effect of large diameters in Eq. (3.3). All three distributions have the dome shape with distinctive breakage occurring at the border diameters that were chosen manually and applied to the droplet data during filtering: *2 mm*, *2.5 mm* and *3 mm* for small, medium and big nozzle correspondingly. Looking at the obtained distributions it can be assumed that during the filtering not only ligaments were excluded from the droplet data, but also some droplets, and, hence, the border diameters might have been set slightly bigger. The second reason why larger droplets are missing in obtained distributions is that they did not create sharp edges on the images as seen in Figure 8.4 (because their diameters might have been bigger than set depth-of-field of the camera).

Default value of spread parameter n in Rosin-Rammler mass fraction frequency distribution in pressure-swirl atomizer model of ANSYS Fluent is equal to *3.5* and can be modified to match the experimental distribution (ANSYS Fluent Theory Guide, 2013, p. 436). Obtained best-fit values of n in Rosin-Rammler droplet volume frequency distributions are *2.21*, *2.31*, *2.51* for small, medium and big nozzle correspondingly (see Table 8.4, 8.6, 8.8).

Droplet velocity frequency distributions are also of interest for calculation of heat and mass transfer between water droplets and vapor in the containment volume and inside pressurizer, as well as between the water droplets and air in spray cooling pond.

Experimental droplet velocity frequency distributions are also presented in the form of histogram, where the bin heights are calculated as a number of droplets which velocities fall between the bin limits. Bin widths are chosen automatically by Excel and equal to *0.42 m/s*, *0.32 m/s*, *0.27 m/s* for small, medium and big nozzle correspondingly.

Droplet velocity frequency and cumulative frequency distributions are illustrated in Figures 8.17, 8.18, 8.19.

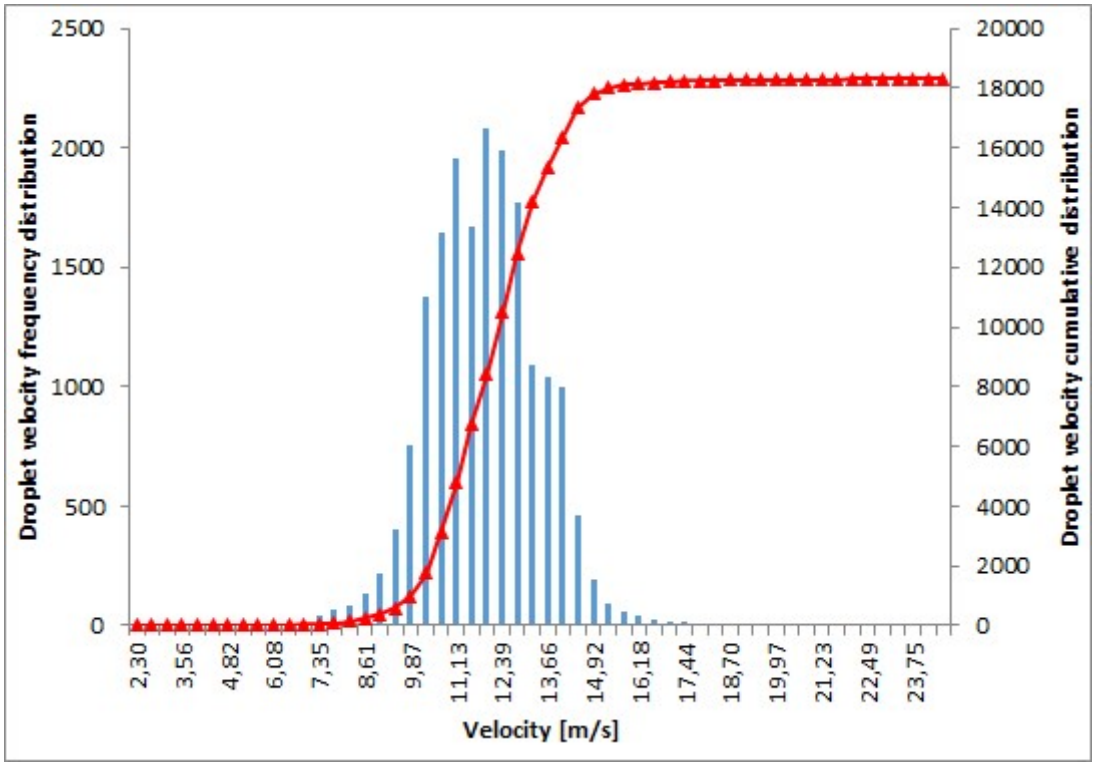

Figure 8.17. Droplet velocity frequency and cumulative distributions for small nozzle.

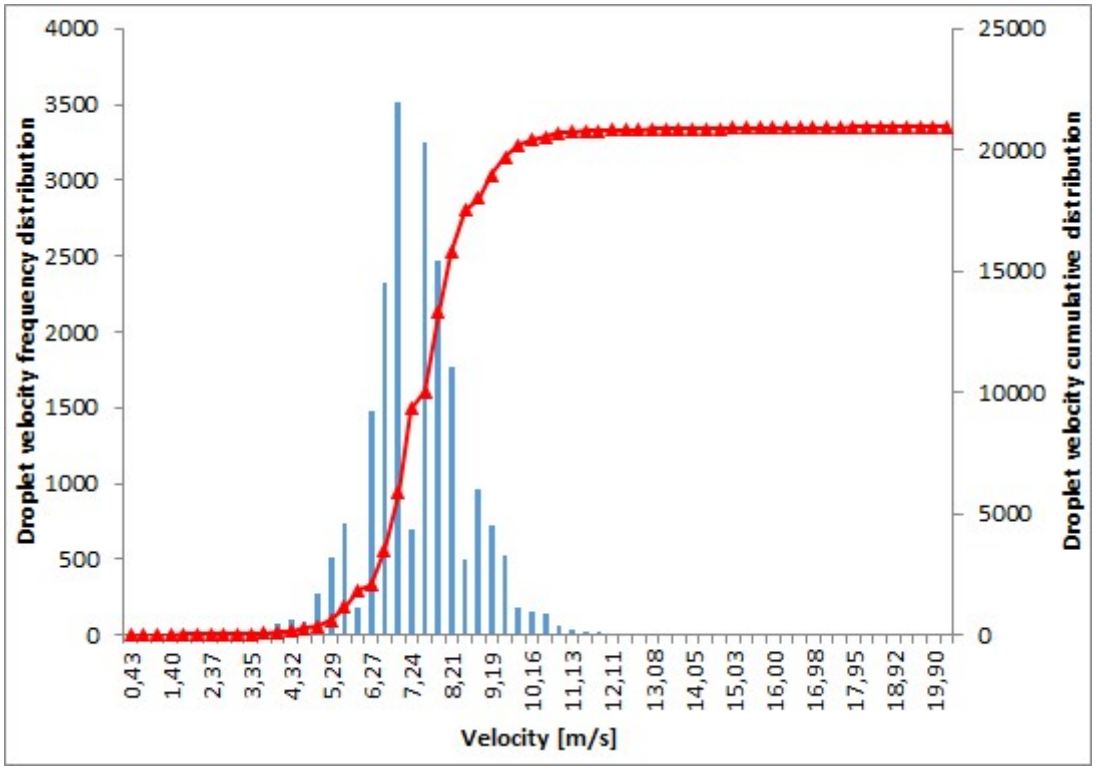

Figure 8.18. Droplet velocity frequency and cumulative distributions for medium nozzle.

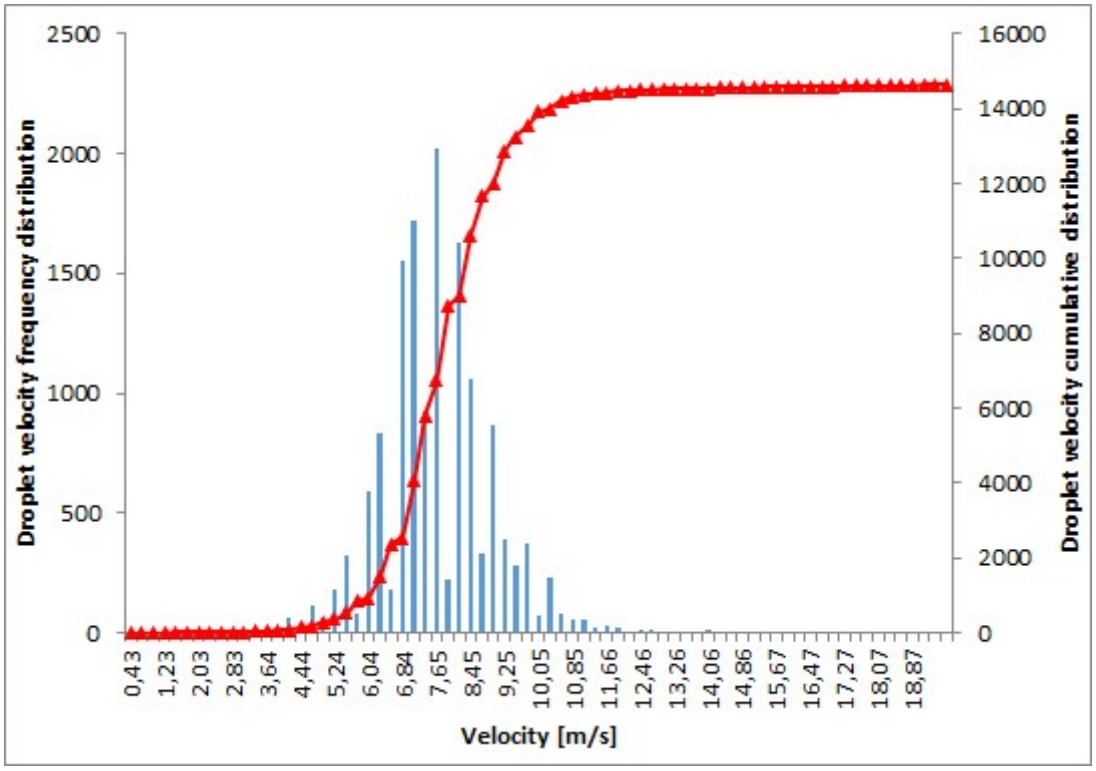

Figure 8.19. Droplet velocity frequency and cumulative distributions for big nozzle.

Notice, that out of 40000 droplets on the first frames used for making statistics and plotting the distributions, DaVis could find pairs only for a certain part of them, namely for 18354, 20980 and 14678 of droplets for small, medium and big nozzle correspondingly.

The reason why DaVis could not find the pairs for many of droplets is that during calibration process, to get the same brightness on both frames, power of laser Pulse A was set to 31% of max whereas that of Pulse B was 13% of max (the reason for such difference is that second frame is inherently exposed for longer time and, thus, requires less laser power). But during the data acquisition this led to the number of droplets detected on the first frames being always bigger than that on the second frames which can be seen both on the processed images and in the droplet data. As a reference, both frames of random image of spray of big nozzle are presented in Figures 8.20, 8.21.

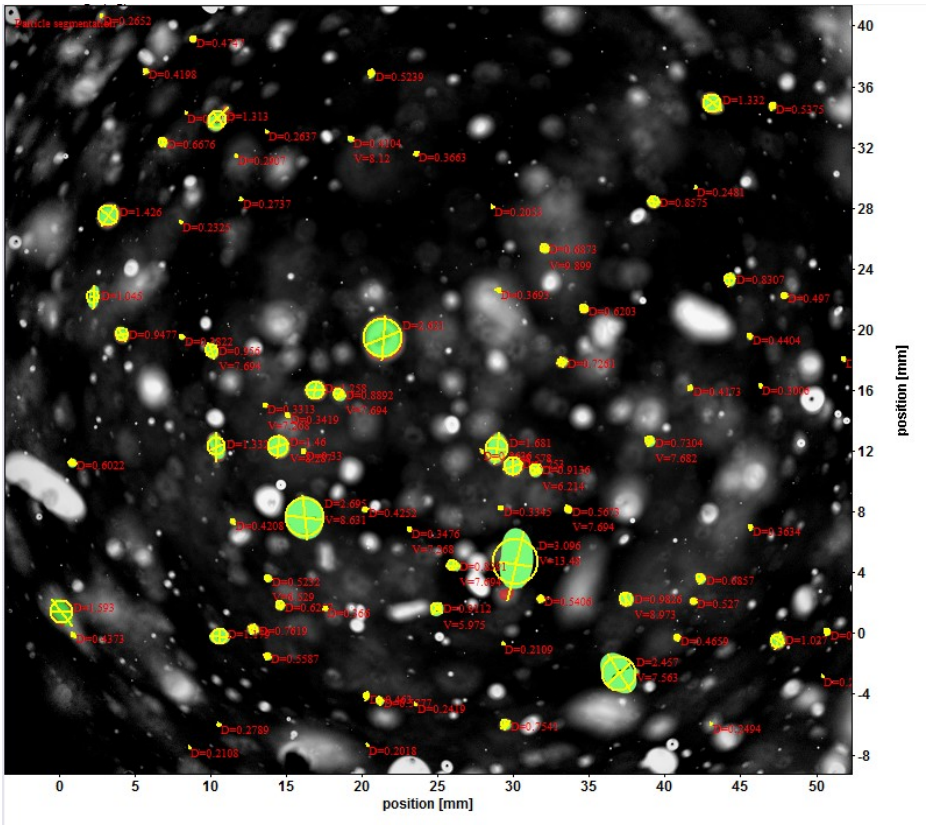

Figure 8.20. First frame of random image of spray of big nozzle.

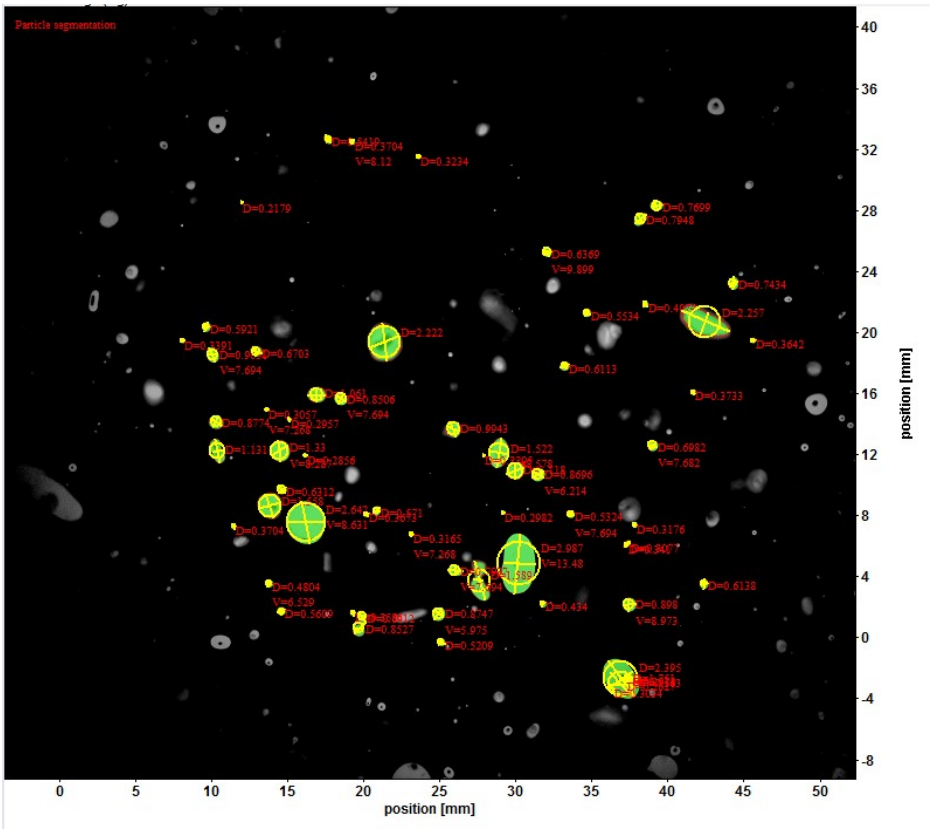

Figure 8.21. Second frame of random image of spray of big nozzle.

According to recommendations given in (LaVision, 2013, p. 14) mean shift between droplets on two frames should be at least 3 pixels and about half the size of the smallest droplet. Calculation of required and experimental mean shifts is presented in Table 8.11.

Table 8.11. Required and experimental droplet shifts.

	Small nozzle	**Medium nozzle**	**Big nozzle**
Diameter of the smallest droplet, D_{min}, mm	*0.19*	*0.19*	*0.19*
Required shift, ($D_{min}/2$), mm	*0.095*	*0.095*	*0.095*
Mean velocity, m/s	*11.8*	*7.3*	*7.4*
Pulse delay time *dt*, μs	*10*	*10*	*10*
Experimental mean shift, mm	*0.118*	*0.073*	*0.074*

Table 8.12 represents numbers of droplets under consideration at different stages of processing.

Table 8.12. Number of droplets under consideration at different stages of processing.

	Small nozzle	**Medium nozzle**	**Big nozzle**
Total number of particles captured	76866	49798	54084
Border diameter for filtering	*2 mm*	*2.5 mm*	*3 mm*
Number of droplets after filtering	76596	49270	53022
Number of ligaments excluded	270	528	1062
Number of droplet pairs detected (out of 40000)	18354	20980	14678

It is seen that default pulse delay time *dt* equal to *10 μs* turned out to be slightly bigger than required for the small nozzle, which assumes that the droplet pairs had a suitable separation; whereas for medium and big nozzles it turned out to be smaller than required. In doing so number of pairs detected for medium nozzle is bigger than for small and big ones. Most likely, the used *dt* turned out to be optimal for the droplet size range presented

in medium nozzle the most. Thus, in the future *dt* should be adjusted separately for each nozzle.

Frequency distributions of velocity are similar in shape to Gaussian distribution. The range of velocities for small nozzle is located in the area of bigger velocities compared to the other two resulting in maximums of distributions being equal to *12.0 m/s*, *6.9 m/s* and *7.4 m/s* for small, medium and big nozzle correspondingly (see Figures 8.17, 8.18, 8.19). Statistical results on droplet velocities are summarized in Table 8.13.

Table 8.13. Statistical results on droplet velocities.

	Small nozzle	**Medium nozzle**	**Big nozzle**
Mean velocity, m/s	*11.8*	*7.3*	*7.4*
St. deviation of mean velocity, m/s	*2.32*	*1.74*	*1.88*

Obviously, mean velocity for small nozzle is higher than for medium and big ones. This is the reason why the values of D_{10}, D_{20} and D_{30} along with dispersion of droplet diameters (featuring by standard deviation of D_{10}) for small nozzle turned out to be the smallest out of three (see Table 8.10, 8.13). The higher the droplet mean velocity in a spray, the more breakups they undergo, which results in wider droplet diameter range and smaller droplets.

DISCUSSION AND CONCLUSIONS

As a result of this work the following points shall be mentioned:

1. Shadowgraphy system was successfully tested;
2. Test bench with single nozzle and necessary measuring instruments was mounted;
3. Pilot experience on installation, calibration and acquisition of droplet data was obtained;
4. Three spray nozzles of different nominal capacities were measured in the air atmosphere at room temperature;
5. Factors influencing the spray droplet sizes in the experiments were analyzed;
6. Droplet size and velocity distributions were obtained;
7. Arithmetic mean and Sauter mean diameters were calculated;
8. Two mathematical models (Rosin-Rammler and Nukiyama-Tanasawa) along with two optimality criteria (*AMAD* and *RSS*) were proposed and applied in order to fit the experimental droplet data;
9. Best-fit values of the fitting parameters for Rosin-Rammler (*n*) and Nukiyama-Tanasawa (*n* and *p*) droplet number and volume frequency distributions were found that made it possible to model the used nozzles in ANSYS Fluent.

It was found that the higher the nozzle capacity, the lower the droplet mean velocity and the larger arithmetic and Sauter mean diameter.

It is seen that Nukiyama-Tanasawa droplet number frequency distributions fit experimental droplet number histograms much better than Rosin-Rammler ones (see Figures 8.11 - 8.13). Nukiyama-Tanasawa fitting is quite accurate in the area of larger diameters, and fitting quality reduces moving to smaller diameters, which is practically acceptable because larger droplets are more important in heat transfer than smaller ones. However, obtained underestimation of number of small droplets would mean more nozzles required to provide adequate heat transfer. Moving from small to big nozzle Nukiyama-Tanasawa fitting improves (value of RSS_N reduces). Therefore, it can be assumed that Nukiyama-Tanasawa droplet number frequency distribution works better for nozzles of coarser atomization. Rosin-Rammler droplet number frequency distribution, in its turn, showed very poor fitting with nozzles studied.

Rosin-Rammler and Nukiyama-Tanasawa droplet volume frequency distributions fit experimental droplet volume histograms with almost the same quality (see Figures 8.14 - 8.16). Both distributions fit experimental results more accurate in the area of smaller diameters, and fitting quality slightly decreases in the area of larger diameters. It can also be noted that fitting quality of both distributions is almost the same through all three nozzles. All in all, it is evident that both distributions can be used interchangeably.

In future droplet size measurements more attention should be paid to depth-of-field of the camera, obtained data gives the grounds to assume that chosen value for it turned out to be small so that larger droplets did not create sharp edges on the images and could not be sized (see Figure 8.4).

In future droplet velocity measurements, more attention should be paid to calibration of brightness between two frames, it needs to be checked for being equal on the captured images after data acquisition (see Figures 8.20 - 8.21). In addition, adjustment of delay time *dt* between two laser pulses should be done separately for each nozzle because of different spray densities they have. The emphasis of this work was put to droplet size measurement, and in order to get good droplet velocity data it is necessary to conduct separate measurements with accurate adjustment and control of all influencing parameters.

REFERENCES

Anon., 1999. *Main equipment of reactor plant.* Moscow, Russia: The Ministry of Atomic Energy of the Russian Federation. Rosenergoatom Concern OJSC. Balakovo NPP. Personnel training service.

Anon., 1999. *Technological systems of reactor plant. Part 1.* Moscow, Russia: The Ministry of Atomic Energy of the Russian Federation. Rosenergoatom Concern OJSC. Balakovo NPP. Personnel training service.

Anon., 2013. *ANSYS Fluent Theory Guide.* Release 15.0. Canonsburg, PA, USA.

Anon., 2013. *ANSYS Fluent User's Guide.* Release 15.0. Canonsburg, PA, USA.

Anon., 2013. *Product manual for DaVis 8.2.* Göttingen, Germany: LaVision.

Anon., 2015. *Industrial hydraulic spray products. Catalog 75A-M HYD.* Wheaton, IL, USA: Spraying Systems Co.

Anon., 2016. *Spray nozzles.* [Online document]. [Accessed 3 August 2016] Available at: http://www.baset.ru/production/forsunki

Ashgriz, N., 2011. *Handbook of atomization and sprays. Theory and Applications.* New York, NY, USA: Springer Science+Business Media, LLC.

González-Tello, P., Camacho, F., Vicaria, J. & González, P., 2008. A modified Nukiyama-Tanasawa distribution function and a Rosin-Rammler model for the particle-size-distribution analysis. *Powder Technology,* September, Issue 186, pp. 278-281.

Lefebvre, A. H., 1989. *Atomization and sprays.* West Lafayette, Indiana, USA: Hemisphere Publishing Corporation.

Lefebvre, A. H., 2011. Atomization. *Thermopedia,* pp. 1-7.

Lefebvre, A. H. & Ballal, D. R., 2010. *Gas Turbine Combustion. Alternative Fuels and Emissions.* 3rd ed. Boca Raton, FL, USA: CRC Press, Taylor & Fransis Group.

Liu, H., 2000. *Science and engineering of droplets. Fundamentals and applications.* Norwich, New York, USA: Noyes Publications / William Andrew Publishing, LLC.

Nasr, G., Yule, A. & Bendig, L., 2002. *Industrial sprays and atomization. Design, analysis and applications..* London, UK: Springer-Verlag.

Pimentel, R. G., 2006. *Doctoral Thesis. Measurement and prediction of droplet size distribution in sprays.* Département de génie mécanique, FACULTÉ DE SCIENCES ET GÉNIE, UNIVERSITÉ LAVAL, QUÉBEC, Canada.

Schick, R. J., 2008. *Spray Technology Reference Guide: Understanding Drop Size.* Wheaton, IL, USA: Spraying Systems Co.

Sirignano, W. A., 2010. *Fluid dynamics and transport of droplets and sprays.* 2nd ed. New York, NY, USA: Cambridge University Press.

Vorobiev V.V, Nemcev V.A, Sorokin V.V & Tyshkevich L.F, 2011. *Effectiveness of Containment Spray System of LSS VVER.* Podolsk, Russia.

Zorin, V. M., 2012. *Nuclear Power Plants, textbook for high schools.* Moscow, Russia: MPEI Publishing House.